Substorm-like magnetospheric response to a discontinuity in the B_x component of interplanetary magnetic field

M. Nowada,[1] C.-H. Lin,[2] Z.-Y. Pu,[1] S.-Y. Fu,[1] V. Angelopoulos,[3] C. W. Carlson,[4] and H.-U. Auster[5]

Received 31 May 2011; revised 19 February 2012; accepted 1 March 2012; published 21 April 2012.

[1] We examined the magnetospheric magnetic field and plasma responses to an encounter of a discontinuity in the B_x component of interplanetary magnetic field (IMF). The striking variations of simultaneous solar wind dynamic pressure and IMF-B_z were not observed. Furthermore, we found that this IMF-B_x discontinuity was a heliospheric current sheet, separating two high-speed solar wind streams with different velocity and magnetic polarity. In this study, the magnetic field and plasma data were obtained from Time History of Events and Macroscale Interactions during Substorms (THEMIS), Cluster, and GOES to investigate the magnetospheric responses, and those were taken from ACE and Geotail to monitor the solar wind conditions. Simultaneous geomagnetic field variations from the ground observatories and aurora activity from Polar were also examined. When the discontinuity encountered the magnetosphere, THEMIS-D, -E, and THEMIS-A observed abrupt and transient magnetic field and plasma variations in the dawnside near-Earth magnetotail and tail-flank magnetopause. Significant magnetic field perturbations were not observed by Cluster as located in the duskside magnetotail at this time interval. Although simultaneous dipolarization and negative bay variations with Pi2 waves were observed by GOES and the ground observatories, global auroral activities were not found. Around the dawnside tail-flank magnetopause, THEMIS-C and -A experienced the magnetopause crossings due to the magnetopause surface waves induced by Kelvin-Helmholtz instability. These results suggest that the magnetic field and plasma variations in the near-Earth magnetotail and tail-flank magnetopause were caused by moderate substorm-like phenomena and magnetopause surface waves. They also indicate that clear magnetospheric disturbances can be brought even without significant variations in the solar wind.

Citation: Nowada, M., C.-H. Lin, Z.-Y. Pu, S.-Y. Fu, V. Angelopoulos, C. W. Carlson, and H.-U. Auster (2012), Substorm-like magnetospheric response to a discontinuity in the B_x component of interplanetary magnetic field, *J. Geophys. Res.*, *117*, A04218, doi:10.1029/2011JA016894.

1. Introduction

[2] Variations of the solar wind conditions cause various physical phenomena in the terrestrial magnetosphere. Substorms in the near-Earth magnetotail and magnetic reconnection at the magnetospheric boundary layer can be triggered by the change of the solar wind conditions [e.g., *Meng and Liou*, 2004]. The magnetospheric responses under various solar wind conditions have been studied based on the magnetic field and plasma data obtained from simultaneous multipoint observations in the solar wind and the magnetospheric regions, and on the ground as well. A global computer simulation also enables us to reproduce the magnetospheric responses for various solar wind conditions. In particular, numerous papers focus on the effect of large-scale interplanetary magnetic field IMF-B_z and solar wind plasma parameter variations associated with magnetic clouds (MC), interplanetary coronal mass ejections (ICME), and corotating interaction regions (CIR) [e.g., *Wilken et al.*, 1998; *Borovsky and Denton*, 2006; *Denton et al.*, 2006; *Zuo et al.*, 2007, 2010, and references therein] or interplanetary shock's (IPS) passage accompanyied by large enhancement of the solar wind dynamic pressure [e.g., *Kokubun et al.*, 1977; *Zhou and Tsurutani*, 2001; *Tsurutani and Zhou*, 2003; *Samsonov et al.*, 2007; *Wang et al.*, 2010, and references therein] on geoeffectiveness.

[3] *Lui et al.* [2008] and *Keika et al.* [2009] revealed global magnetic field and plasma variations in the inner magnetosphere in association with simultaneous substorm and magnetopause motion (or related surface waves) from

[1]Institute of Space Physics and Applied Technology, School of Earth and Space Sciences, Peking University, Beijing, China.
[2]Department of Electrical Engineering, Ching Yun University, Taoyuan, Taiwan.
[3]Institute of Geophysics and Planetary Physics, University of California, Los Angeles, California, USA.
[4]Space Sciences Laboratory, University of California, Berkeley, California, USA.
[5]Institut für Geophysik und Extraterrestrische Physik, Technische Universität, Braunschweig, Germany.

0148-0227/12/2011JA016894

the multispacecraft observations. With only information obtained from a single spacecraft, the phenomenon occurring at the local point can be clarified, but questions like, "What is the physical source for this phenomenon and "how associated phenomenon was observed" are still difficult to be answered.

[4] In order to identify an occurrence of a substorm, it becomes a key point to examine whether the following four phenomena are observed or not in the magnetosphere and on the ground: (1) the dipolarization process as indicated by an enhancement of the northward magnetic field component, (2) simultaneous magnetic field stretching shown as an enhancement of the sun-earthward magnetic field component, (3) MHD waves at the Pi2 range with a period (frequency) is from 40 s to 150 s (6.7 mHz to 25 mHz), and (4) associated global and/or local auroral activities. The observed event might not be identified as a "pure" substorm process, unless these four phenomena were all observed by the satellites and ground observatories [cf. *Akasofu et al.*, 2010, 2011; *Feldstein et al.*, 2011].

[5] The motion of the magnetospheric boundary layer and the waves on the boundary surface are frequently caused by the external drivers, such as variations of the solar wind dynamic pressure and the orientation of the IMF-B_z component. Due to the variations of the solar wind conditions, the pressure balance between the magnetic pressure in the magnetosphere and the solar wind dynamic pressure is lost. For instance, the magnetopause is pushed inward from its normal position where the magnetic and dynamic pressures are well balanced to the magnetospheric site under high solar dynamic pressure. The magnetopause begins to move toward the solar wind site to return its location to the normal position when the dynamic pressure becomes low. These frequent inward and outward motions would be one of the possible mechanisms to generate magnetopause surface waves [*Matsuoka et al.*, 1993; *Kepko et al.*, 2002; *Kepko and Spence*, 2003].

[6] When the IMF-B_z is southward, the magnetopause position could also move inward from its normal location due to the magnetic reconnection (erosion) at low-latitude dayside magnetopause. During dayside magnetic reconnection (erosion), merged magnetic field lines are transported into the magnetotail by the solar wind, and the geomagnetic field lines could trap the newly penetrating solar wind plasma. As a result, new magnetopause is formed at a deeper location in the magnetosphere than the normal magnetopause position. When the reconnection (erosion) stops, the magnetopause returns to its normal position. This imbalance due to the magnetic reconnection (erosion) causes the magnetopause motion and associated surface waves [e.g., *Aubry et al.*, 1970; *Wiltberger et al.*, 2003].

[7] Another candidate to generate surface waves is Kelvin-Helmholtz instability (KHI). Based on in situ satellite observations, KHI is favorable to occur on the magnetopause in the magnetotail flank region where a velocity shear between the solar wind high speed streams and magnetosphere stagnant flows is large [*Sckopke et al.*, 1981; *Fujimoto et al.*, 1998; *Fairfield et al.*, 2000]. Furthermore, the sudden and/or moderate changes in the solar wind conditions, such as the dynamic pressure and/or IMF orientation, are not required for the KHI to grow at the magnetopause, although KHI is likely to grow under the northward IMF-B_z periods [e.g., *Fujimoto et al.*, 1998; *Hasegawa et al.*, 2004, 2006]. Based on the Cluster observations, *Hasegawa et al.* [2004] estimated that the size of the vortex induced by KHI could reach about 6.0 RE $\sim$ 9.0 RE in the case of the velocity shear layer with the thickness between about 0.8 RE and 1.1 RE. Resultant magnetopause thickness (as a proxy parameter of the disturbance scale) was about 3.1 RE $\sim$ 4.4 RE. The study based on the three-dimensional MHD computer simulation performed by *Takagi et al.* [2006] also supported that the vortex size (wavelength) induced by KHI was approximately 8 times the velocity shear layer. Accordingly, KHI is a physical mechanism that could generate magnetopause surface waves.

[8] In this study, we obtain a global view for the magnetic field and plasma responses in the near-Earth magnetotail and tail-flank magnetopause due to an encounter of a sharp magnetic discontinuity in the IMF-B_x component on 25 November 2007. An observed discontinuity was not associated with an enhancement of the solar wind dynamic pressure and large southward IMF-B_z structure. This study is conducted based on the magnetic field and plasma data obtained from simultaneous observations in the solar wind and magnetosphere by the nine satellites. Although the substorm is hard to be triggered under these solar wind conditions, the observations from the geosynchronous satellites and the ground observatories provide clear evidence for an occurrence of "substorm-like" phenomena due to a passage of the IMF discontinuity. Simultaneous observations from the four THEMIS probes, which were located in the dawnside magnetosphere, detected associated magnetospheric and boundary layer magnetic field and plasma responses.

[9] The paper is organized as follows. Section 2 presents the instrumentation on board the THEMIS spacecraft which monitors the magnetospheric and magnetopause magnetic field and plasma responses due to an encounter of the discontinuity. The detailed observations in the solar wind, the magnetosphere, the magnetopause, and the ground observatories are presented in sections 3–10. The discussion and conclusions are presented in 11sections and 12.

2. Instrumentation on Board THEMIS

[10] The THEMIS spacecraft consists of five probes launched on 17 February 2007, in order to reveal the spatial-temporal structures of magnetospheric processes [*Angelopoulos*, 2008]. In this study, we used the magnetic field data obtained from the fluxgate magnetometers (FGM) that are capable of measuring the low-frequency fluctuations up to 64 Hz, and detecting the magnetic field variations within an accuracy of $\pm$0.01 nT [*Auster et al.*, 2008]. Also, we used the plasma moment data from the electrostatic analyzer (ESA) with the observable range for ions between 0.006 keV/q and 20 keV/q [*McFadden et al.*, 2008] on board all five probes of the THEMIS spacecraft. The time resolutions of both magnetic field and plasma moment data are 3 s.

3. Satellite Locations on 25 November 2007

[11] Figures 1a and 1b show the locations of nine satellites used in this study, projected onto respective XY and XZ planes in the geocentric solar magnetospheric (GSM)

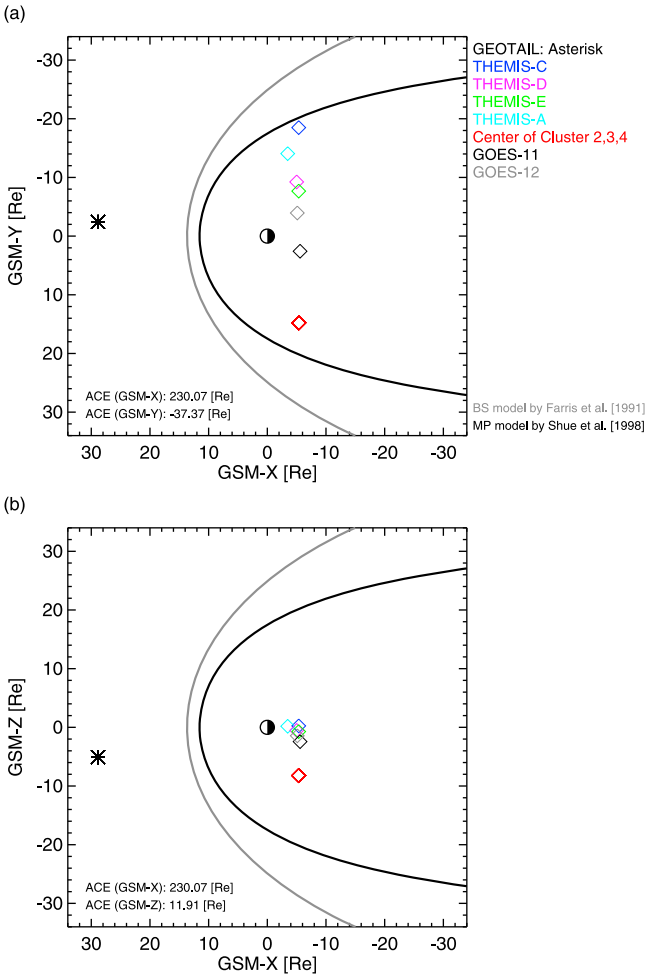

Figure 1. The nine satellite locations projected onto the (a) GSM-XY and (b) -XZ planes at 07:06 UT on 25 November 2007 are presented. The position of Geotail, which was monitoring the solar wind conditions, is shown with an asterisk. The locations of THEMIS-C, -D, -E, -A, and Cluster, which were staying in the dawnside and duskside near-Earth magnetotail, are shown with respective blue, magenta, green, cyan, and red diamonds. Black and gray diamonds show the positions of GOES-11 and -12, respectively. The model bow shock [*Farris et al.*, 1991] shown with the gray curve and magnetopause [*Shue et al.*, 1998] as indicated by the black solid curve are superimposed in the two plots, respectively.

coordinate system on 25 November 2007. The satellite locations at 07:06 UT, when THEMIS observed the initial magnetospheric magnetic field and plasma responses, are shown with the colored diamonds. The model bow shock [*Farris et al.*, 1991] and magnetopause [*Shue et al.*, 1998] are superimposed, respectively. The THEMIS-D (magenta) and -E (green) probes were located very close to each other, and staying in the dawnside near-Earth tail region. Simultaneous THEMIS-C (blue), and -A (cyan) probes were located at respective outer (magnetosheath) and inner (magnetosphere) sites of the dawnside tail-flank magnetopause.

[12] In order to examine the corresponding magnetic field variations in the opposite duskside magnetotail, we utilized the magnetic field data taken from the Cluster satellite (C2, C3 and C4). A plotted position (red) is the center of the three Cluster's probes. Cluster was just located in the opposite duskside near-Earth magnetotail and the Southern Hemisphere (GSM-Z $\sim$ -8 RE). The magnetic field data from GOES-11 and -12 were also used to examine the nightside magnetic field variations at geosynchronous altitudes to clarify whether the THEMIS's magnetic field and plasma variations were related to the phenomena in the near-Earth tail. The positions of GOES-11 (black) and -12 (gray) were at the pre-midnight (about 22 h $\sim$ 23 h magnetic local time (MLT)) and the pre-dawn (about 4 h $\sim$ 5 h MLT) magnetospheric sectors, respectively. All THEMIS's probes and two GOES satellites were almost on the magnetic equatorial plane. The GSM-X positions of these 7 satellites which stayed in the magnetotail were almost within the range between -7 RE and -9 RE.

[13] ACE and Geotail were located at 230 RE upstream from the earth, and about 30 RE in the sunward away from the earth in GSM-X as shown with asterisk, respectively. The distance between ACE and Geotail in GSM-Y and -Z was 35 RE and 17 RE, respectively. Both of them were located in the dawnside, but Geotail was closer to the magnetic equatorial plane than ACE.

4. Solar Wind Conditions

4.1. Overview of Solar Wind Observations by ACE and Geotail

[14] The plots of the solar wind conditions during 1 h and 40 min from 06:30 UT to 08:10 UT obtained by ACE and Geotail are shown in Figure 2. The top six plots show the three components of the IMF (B_x, B_y and B_z) in GSM coordinate system, the plasma number density (N_p), the solar wind bulk flow velocity (V_{sw}) obtained from ACE, and the solar wind ram (dynamic) pressure (P_d) calculated with a formula of $mN_pV_{sw}^2$, where "m" is the mass of the ion, respectively. The bottom six plots show the three components of the IMF in GSM coordinates, the number density, the solar wind velocity and ram (dynamic) pressure obtained from the Geotail measurements, respectively. The ACE and Geotail data were plotted with time shifts of respective about 30 and 5 min of the solar wind time delays so that they coincide with the THEMIS's data-plotting timescale. Here we used the plasma moment data measured by the Energetic Particle and Ion Composition Instrument (EPIC) on board Geotail (details are given by *Williams et al.* [1994]).

[15] ACE observed a sharp magnetic field change (magnetic field discontinuity) from positive to negative in the B_x component at the time interval marked with "A." The 8.5 min duration bracketed by two black broken lines with the two-headed arrow is the corresponding time interval when THEMIS-A observed the magnetospheric abrupt and transient magnetic field and plasma variations. Simultaneous B_y and B_z components did not show the drastic changes as seen in the B_x component. The solar wind bulk speed and simultaneous plasma density clearly decreased from 600 km/s to 570 km/s, and from 3.25/cc to 2.50/cc in association with a sharp B_x discontinuity, respectively. These parameters did not show the significant changes except for the discontinuity interval. The associated ram (dynamic) pressure also decreased from 2.0 nPa to 1.4 nPa, but had been almost

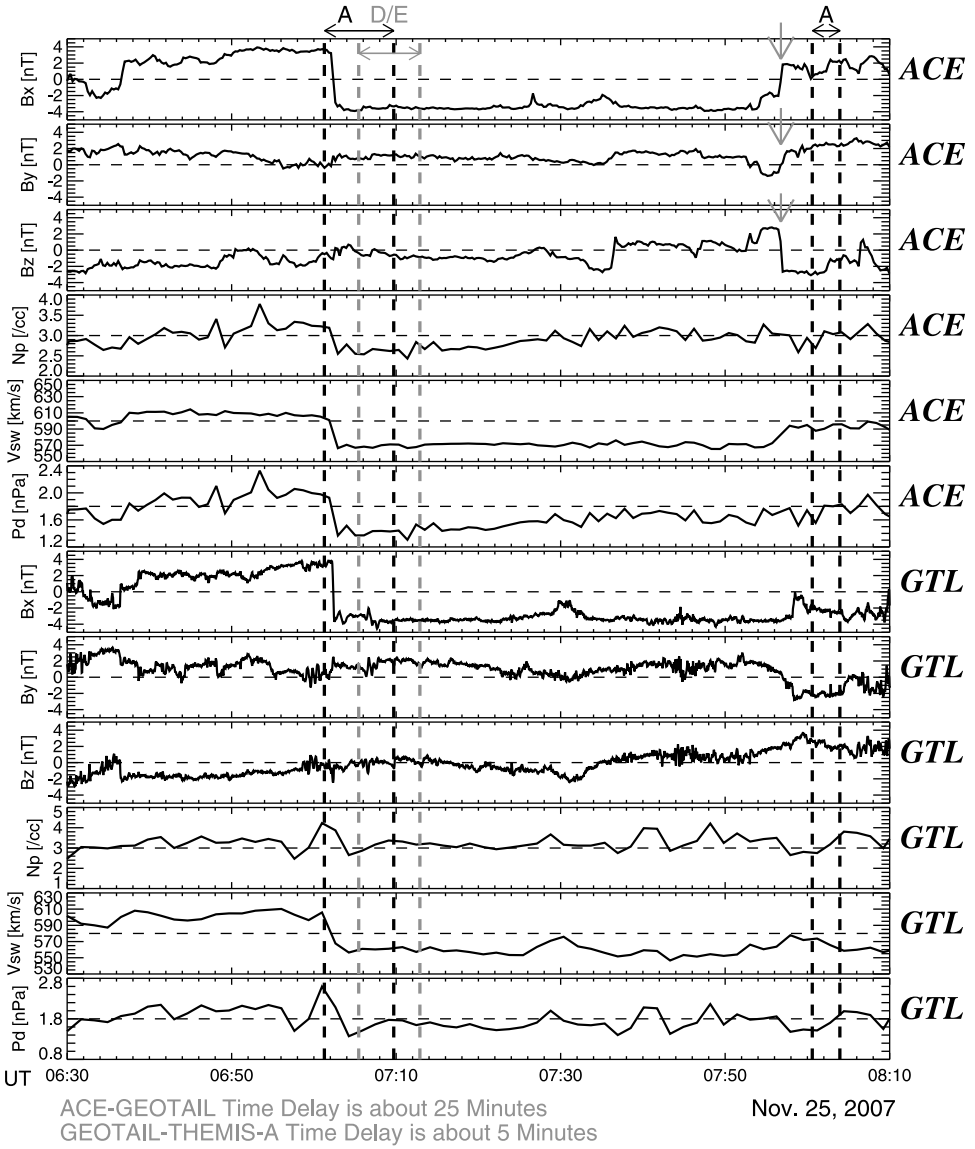

Figure 2. Solar wind conditions from 06:30 UT to 08:10 UT as obtained by ACE and Geotail are presented. The top six plots present the three components of the IMF (B_x, B_y and B_z) in GSM coordinate system, the plasma number density (N_p), the solar wind bulk flow velocity (V_{sw}) and the solar wind ram (dynamic) pressure (P_d) obtained from the ACE measurements, respectively. The bottom six plots present the three components of the IMF in GSM coordinates, the number density, the solar wind velocity and ram (dynamic) pressure taken from the Geotail measurements, respectively. The ACE and Geotail data were plotted with time shifts of about 30 and 5 min, respectively, of the solar wind time delays so that they coincide with the THEMIS's data-plotting timescale. The time intervals corresponding to the abrupt and transient magnetospheric magnetic field and plasma variations observed by THEMIS-A and THEMIS-D/-E are bracketed by two black and gray broken lines with two-headed arrows, respectively. The gray arrows show the second magnetic discontinuity, having the total different magnetic field structures from the first magnetic discontinuity.

stable during the whole interval. The average ram (dynamic) pressure was about 1.6 nPa.

[16] Geotail also observed the clear discontinuity of the IMF-B_x component with the positive-to-negative polarity reversal 25 min later since ACE observed it. This sharp magnetic field discontinuity was shown only in the B_x component, and no particular variations were observed in both B_y and B_z components as well as those by the ACE's measurements. When a sharp B_x discontinuity was observed, the orientations of the B_y and B_z components were duskward and weakly southward, respectively. Also, the solar wind velocity and plasma density showed a clear decrease from 600 km/s to 550 km/s, and from 4.0/cc to 2.6/cc, respectively. Resultant solar wind ram (dynamic) pressure decreased from 2.6 nPa to 1.4 nPa.

[17] Based on the solar wind observations by ACE and Geotail, the magnetic discontinuity was observed in a high-speed solar wind stream whose average velocity is about 600 km/s. At the B_x discontinuity, the solar wind velocity clearly decreased. Therefore, the discontinuity is an interface/boundary between two high-speed streams with different velocity and magnetic polarity. These two streams should be separated by heliospheric current sheet (HCS). The observed density drop seen at the discontinuity is evidently related to a rarefaction in the solar wind stream after the faster stream has passed. About 5 min later since Geotail detected the discontinuity, THEMIS-A observed the abrupt and transient magnetic field and plasma variations in the dawnside near-Earth magnetotail.

[18] Next 7.5 min bracketed by two gray broken lines marked as "D/E" with the two-headed arrow are corresponding time interval when THEMIS-D/-E observed the magnetospheric abrupt and transient magnetic field and plasma variations. Note that there was about 4 min time delay for the observations of the abrupt and transient magnetic field and plasma variations between THEMIS-A and THEMIS-D/-E. During this time interval, ACE did not observe significant variations for the IMF, the plasma parameter and the ram (dynamic) pressure. Also, Geotail did not detect the IMF and the solar wind velocity changes, but simultaneous plasma density and ram (dynamic) pressure were recovering the background levels after the magnetic discontinuity, respectively.

[19] About 1 h later since a sharp B_x discontinuity was observed, again, ACE observed the other sharp magnetic field changes with the polarity reversal in all components of the IMF as shown with gray arrows. The B_x component changed its polarity from negative to positive, and simultaneous B_y and B_z components changed from negative to positive and from positive to negative, respectively. Simultaneous plasma number density and ram (dynamic) pressure did not change, but only solar wind velocity slightly enhanced from 570 km/s to 590 km/s. Therefore, an observed discontinuity should also be HCS which is separating two high-speed streams with different velocity and magnetic polarity. Geotail observed it with further time delay about 15 min or 20 min (not shown during the presented data-plotting timescale). The slight enhancements of the plasma density and ram (dynamic) pressure, but no clear variation were observed in the solar wind velocity with Geotail.

[20] THEMIS-A observed the abrupt and transient magnetic field and plasma variations 3 min later since the second magnetic discontinuity was observed by ACE. The corresponding 3.5 min interval is bracketed by two black broken lines marked as "A" with the two-headed arrow. Due to further time delay for an observation of the second magnetic discontinuity between ACE and Geotail, the polarities of all IMF components observed by ACE were just opposite to those by Geotail. Simultaneous THEMIS-D/-E did not observe any striking variations for both magnetic field and plasma in the near-Earth magnetotail.

4.2. Detailed Magnetic Field and Plasma Structures of the IMF-B_x Discontinuity

[21] In order to clarify the features of this sharp magnetic discontinuity, we investigated the detailed variations of the magnetic field seen in the frame of reference fixed at the discontinuity surface, and the plasma with a zoom-in plot. Figure 3 shows the 30 min interval plot between 06:18 UT and 06:48 UT of the magnetic field and plasma data obtained from ACE. From top to bottom, the plots present the three components of the magnetic field in LMN coordinates, determined by minimum variance analysis (MVA) [e.g., *Sonnerup and Cahill*, 1967; *Russell and Elphic*, 1978], the number density, the solar wind velocity (V_x), the total pressure (P_{tot}), which is a summation of the solar wind magnetic and plasma pressures calculated with a formula of $\frac{1}{2\mu_0}B_t^2 + N_p k T_p$, where respective μ_0, B_t, k and T_p are permeability of free space, the IMF intensity, Boltzmann constant and the ion temperature in the solar wind, the solar wind ram (dynamic) pressure, respectively. The matrix to transform LMN from GSM coordinates was made based on the magnetic field data between 06:32:00 UT and 06:34:00 UT. We show the normal vector of the magnetic discontinuity surface obtained by MVA (N_x, N_y, N_z), and the angles between the normal vector onto GSM-XY plane (N_{xy}) and GSM-X axis (θ_{Nxy}), and between that onto GSM-XZ plane (N_{xz})and GSM-Z axis (θ_{Nxz}) in Table 1, respectively. The θ_{Nxy} and θ_{Nxz} were obtained with the formula of $\tan^{-1}\left(\frac{N_y}{N_x}\right)$ and $\tan^{-1}\left(\frac{N_x}{N_z}\right)$, respectively. These results suggest that the magnetic discontinuity was lying with the normal vector oriented to the earth-dawnward and the earth-southward in the GSM-XY and -XZ planes. ACE encountered the magnetic discontinuity at about 06:33:01 UT, bracketed by two gray broken-dotted lines, and during which THEMIS-A observed corresponding magnetic field and plasma variations as shown with two black broken lines. A sharp positive-to-negative discontinuity appeared in the B_L component, but the other B_M and B_N components did not show striking variations during an encounter of the discontinuity. In GSM coordinates, the magnetic discontinuity appeared in the B_x component, that is, the variations of the B_L component are corresponding to those of the B_x component. Furthermore, the fluctuations of the B_M and B_N components were almost similar to those of the B_y and B_z components, respectively.

[22] The plasma density and its velocity respectively decreased from 3.2/cc to 2.5/cc, and from 600 km/s to 575 km/s at the magnetic discontinuity. Simultaneous solar wind ram (dynamic) pressure resulted in decreasing from 1.9 nPa to 1.4 nPa, although total pressure was stable. During the THEMIS-D/-E time interval as bracketed by two gray broken lines, no particular variations were found in the magnetic field, plasma parameters, the total and solar wind ram (dynamic) pressures.

[23] The B_L component, which is the tangential magnetic field component to an IMF discontinuity, showed a clear jump at a discontinuity. The normal magnetic field component (B_N) was nearly zero, and did not show a significant variation across an IMF discontinuity. Furthermore, evident reductions were seen in associated plasma parameters, such as the plasma velocity and number density at a discontinuity. The total pressure had been stable not only across an IMF discontinuity but also during the whole time interval. From these magnetic field and plasma aspects, and the absence of significant total pressure variation, an observed discontinuity

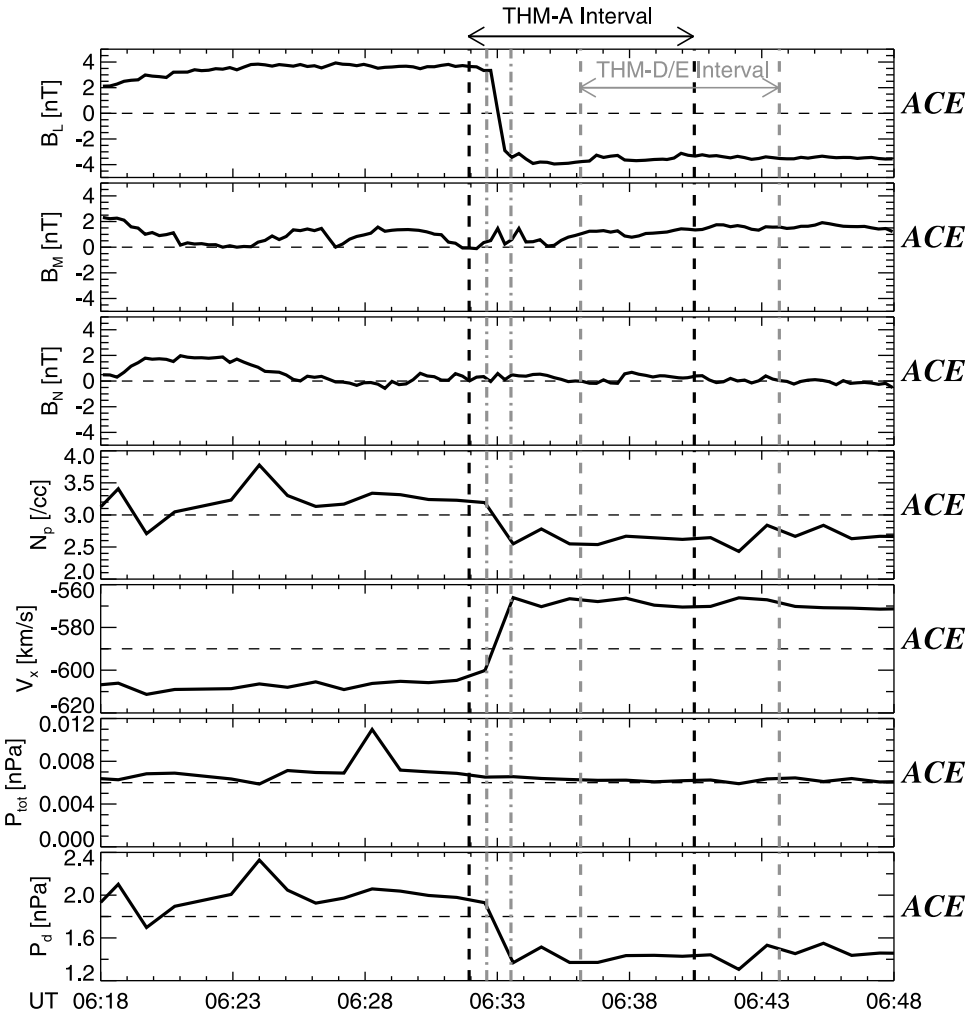

Figure 3. A zoom-in plot during the 30 min interval between 06:18 UT and 06:48 UT of the magnetic field and plasma data obtained from ACE is presented. From top to bottom, the plots show the three components of the IMF in LMN coordinates as determined by MVA, the number density, the solar wind velocity (V_x), the total pressure (P_{tot}), which is a summation of the solar wind magnetic and plasma pressures, and the solar wind ram (dynamic) pressure, respectively. The time interval of an encounter of ACE's magnetic discontinuity is bracketed by two gray broken-dotted lines. The time intervals when THEMIS-A and THEMIS-D/-E observed the magnetospheric magnetic field and plasma responses are also indicated by two black and gray broken lines, respectively.

in the IMF-B_x component obviously indicates the physical features of the tangential discontinuity.

[24] In section 5, we report magnetic field and plasma responses due to an encounter of IMF-B_x discontinuity with the magnetosphere by THEMIS.

5. Magnetic Field and Plasma Variations at the Inner and Outer Sites of the Dawnside Tail-Flank Magnetopause

[25] Figure 4 presents the summary plots of the magnetic field and plasma data obtained from THEMIS-A (black) and -C (gray) during 1 h and 40 min interval from 06:30 UT to 08:10 UT. From top to bottom, the plots show the three components of the magnetic field in GSM coordinates, the magnetic field intensity, the three components of the plasma velocity in GSM coordinates, the plasma number density, and temperature with the universal time (UT), respectively. Unfortunately, the plasma velocity data of THEMIS-C were not available during this interval. The two time intervals during the THEMIS-A observations for the abrupt and transient magnetic field and plasma variations are bracketed by two black solid lines. The peaks for the magnetic field andplasma impulses are shown with black dotted lines with the labels of UT (07:06 UT and 08:03 UT).

Table 1. Normal Vector of the Solar Wind Magnetic Discontinuity Surface and the Angles Between the Discontinuity's Normal Vectors on GSM-XY and -XZ Planes and GSM-XZ Axes

(N_x, N_y, N_z)	θ_{Nxy} (deg)	θ_{Nxz} (deg)
(−0.1773, −0.8121, −0.5560)	−102.32	−162.31

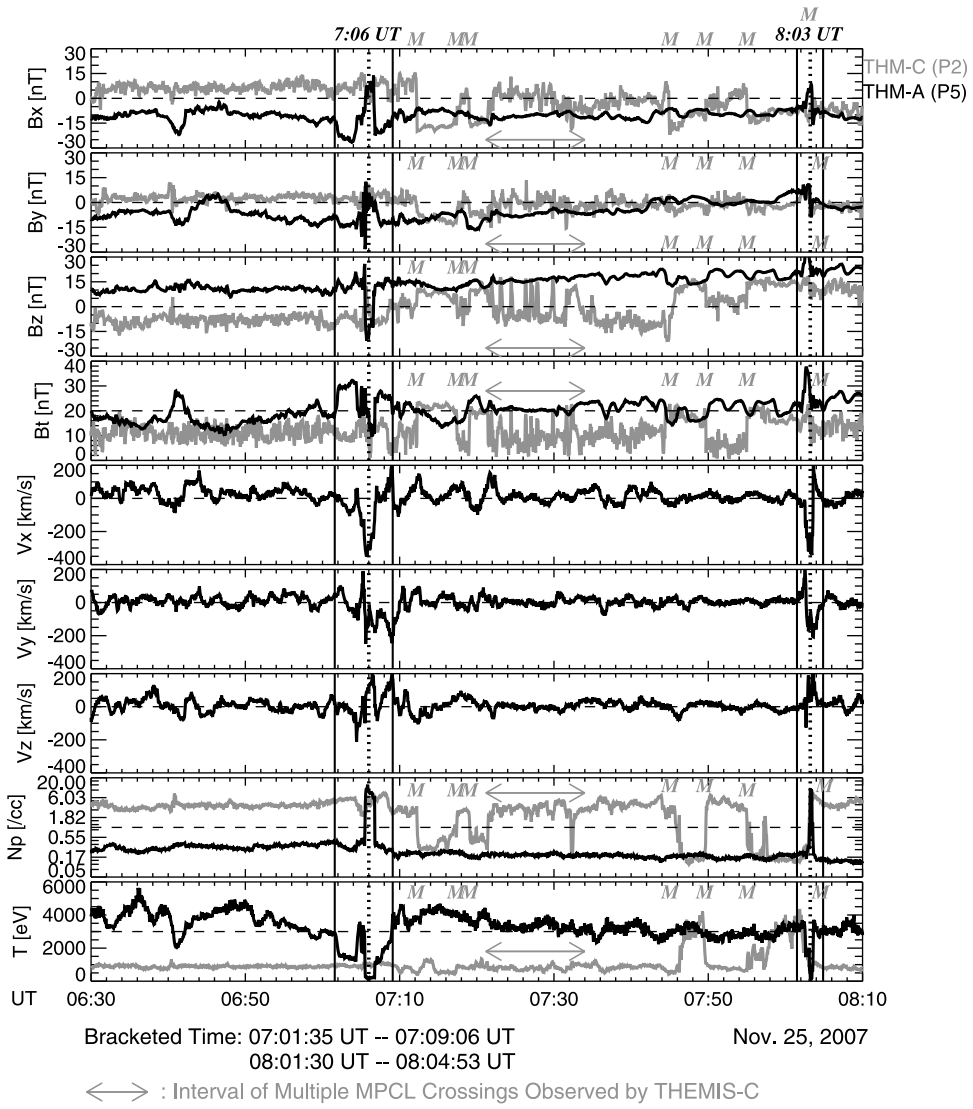

Figure 4. The summary plots of the magnetic field and plasma data obtained from THEMIS-A and -C during 1 h and 40 min interval from 06:30 UT to 08:10 UT are presented. From top to bottom, the plots show the three components of the magnetic field in GSM coordinates, the magnetic field intensity, the three components of the plasma velocity in GSM coordinates, the plasma number density, and temperature plotted with universal time (UT), respectively. The plasma velocity data of THEMIS-C were not available during this interval. The two observational intervals of THEMIS-A for the abrupt and transient magnetic field and plasma variations are bracketed by two gray broken lines. The first time interval is 8.5 min from 07:01:35 UT to 07:09:06 UT, and the second one is about 3.5 min from 08:01:30 UT to 08:04:53 UT. The peaks for the magnetic field and plasma impulses are shown with black dotted lines with the labels of UT (07:06 UT and 08:03 UT).

5.1. THEMIS-A Observations From 07:01:35 UT to 07:09:06 UT

[26] THEMIS-A first detected the variations of both magnetic field and plasma during 8.5 min from 07:01:35 UT to 07:09:06 UT. During this time interval, the B_x component negatively increased its value from −12 nT to −25 nT, and showed successive abrupt variation from −25 nT to +8 nT. After these variations, the value of the B_x component gradually recovered the background magnetic field level (about −10 nT). The B_y component indicated the positive impulsive perturbation (referred to as "positive impulse") followed by the negative impulsive variation (referred to as "negative impulse") between about −30 nT and near +15 nT. Simultaneous B_z component showed the negative impulse from +25 nT to −20 nT, and variation of the B_t reflected well to that of simultaneous B_x component.

[27] Associated V_x component had the negative impulse, and other two velocity components showed the positive impulses. Just before the peaks of the impulses, all plasma velocity components became negative. However, the V_x and V_z components presented the positive impulses, but V_y component showed the negative impulse after their peaks. All velocity components recovered the background level of

the plasma velocity as fluctuating around 0 km/s after the successive positive/negative impulses.

[28] Interestingly, the variations of the plasma number density and temperature were mutually different. The number density showed clear positive impulse associated with the abrupt and transient variations in the magnetic field and plasma velocity. The number density at the peak of the impulse was about 16.5/cc. However, the variation of the simultaneous temperature seemed to have two stages. The abrupt decrease from 3000 eV to 1500 eV was shown at the first stage, and the second one more abruptly decreased from 3300 eV to around 200 eV than the first stage decrease. After the two stages of temperature decrease, the temperature recovered the background level (about 3000 eV) and had showed no striking variations until 08:01:30 UT when the second magnetic field and plasma positive/negative impulses appeared. The first temperature abrupt decrease was corresponding to the enhancement of the magnetic field intensity (B_t) and the negative impulses in all plasma velocity components, but no associated variation was found in the plasma number density. The second one was corresponding to the positive/negative impulses in the magnetic field, the plasma velocity and the plasma number density.

5.2. THEMIS-A Observations From 08:01:30 UT to 08:04:53 UT

[29] The abrupt and transient magnetic field and plasma variations were also observed during about 3.5 min interval from 08:01:30 UT to 08:04:53 UT. The time interval for these variations was shorter than that in the previous event. The B_x component showed the positive-to-negative impulse, but the amplitude of the positive impulse part was much smaller than that of the previous one. The polarities of impulses in simultaneous B_y and B_z components were positive-to-negative and positive, respectively. Their amplitudes, however, were smaller than those in first impulse. The B_t also showed the impulse positively, but the amplitude was almost the same as that in the previous event.

[30] Associated all plasma velocity components presented "bipolar-type" perturbations. The variations with the positive followed by negative were seen in the V_x and V_z components. The V_y component showed the negative followed by positive variation. These "bipolar" perturbations seen in the plasma velocity are observational evidence for the magnetopause surface waves [e.g., *Sibeck*, 1992; *Sibeck and Smith*, 1992]. There was clear anti-correlation between simultaneous number density with a sharp positive impulse and temperature showing the negative impulse. The complicated temperature variations as seen in the previous event were not found here.

[31] The magnetic field and plasma variations during the same time interval in the outer site of the tail-flank magnetopause, observed by THEMIS-C were presented in section 5.3.

5.3. THEMIS-C Observations: A Comparison With THEMIS-A Observations

[32] THEMIS-C observed highly magnetic field and plasma fluctuations during the whole time interval. These variations should be associated with the crossings of the tail-flank magnetopause by THEMIS-C. We then identified the magnetopause crossings experienced by THEMIS-C based on particular variations (jumps) of the B_z component caused by the Chapman-Ferraro boundary current, and associated plasma variations. The magnetopause crossings were denoted by the letters of "M." During particular time interval between 07:21:10 UT and 07:34:00 UT indicated by the two-headed arrow, THEMIS-C experienced the multiple magnetopause crossings. THEMIS-C observed the small amplitude magnetic field and plasma perturbations, when THEMIS-A observed the abrupt and transient magnetic field and plasma variations. At 07:12 UT, the amplitudes of all magnetic field components, field intensity and plasma density became larger than those of the magnetic field and plasma variations at 07:06 UT. This difference of the amplitude for the variations strongly depends on whether the probe "completely" transits from the outer (inner) to inner (outer) site of the tail-flank magnetopause. Therefore, THEMIS-C was "partially" crossing the magnetopause, that is, the probe did not completely transit the magnetosphere from the magnetosheath at 07:06 UT. However, after 6 min, THEMIS-C experienced the "complete" crossing (transition) of the magnetopause. After 07:12 UT, all magnetic field components, the plasma density and temperature were highly fluctuating due to the THEMIS-C's multiple magnetopause crossings.

[33] Comparing the two magnetic field and plasma variations at 07:06 UT and 07:12 UT observed by THEMIS-A with those by THEMIS-C, the values and orientations of particular magnetic field observed by THEMIS-C were almost consistent with those by THEMIS-A. This result strongly suggests that THEMIS-A experienced two intermittent outbound (from inner to outer site of) magnetopause crossings. Also, the peak values of the THEMIS-A's number density and temperature at the two impulses were almost consistent with those of THEMIS-C. To double-check whether THEMIS-A saw the magnetosheath plasma during the time interval of the abrupt and transient plasma variations, we examined simultaneous spectrograms for the time variation of the ion and electron energy (E-t diagrams) obtained from THEMIS-A and -C (not shown here). The energy levels of plasma at the impulses observed by THEMIS-A were almost the same as those in the magnetosheath as seen by THEMIS-C, explicitly suggesting that THEMIS-A transiently and abruptly observed the magnetosheath plasma.

[34] The magnetic field and plasma peak values at two impulsive variations were almost consistent with those of THEMIS-C. Therefore, THEMIS-A experienced the intermittent magnetopause crossings due to the magnetopause motions or surface waves. In section 5.4, based on the detailed analysis for the transient and abrupt magnetic field and plasma variations, we investigate and report what the driving mechanism for the magnetopause motion or surface waves is.

5.4. Detailed Analysis on the Magnetic Field and Plasma Structures From 07:01:35 UT to 07:09:06 UT

[35] In order to clarify the driving mechanism of the magnetopause motion or surface waves that caused the abrupt and transient magnetic field and plasma variations, we tried to investigate the magnetic field and plasma data more detailed. Figure 5 is a zoom-in plot of the magnetic field and plasma data from THEMIS-A in LMN coordinates, which are transformed from GSM based on the MVA during

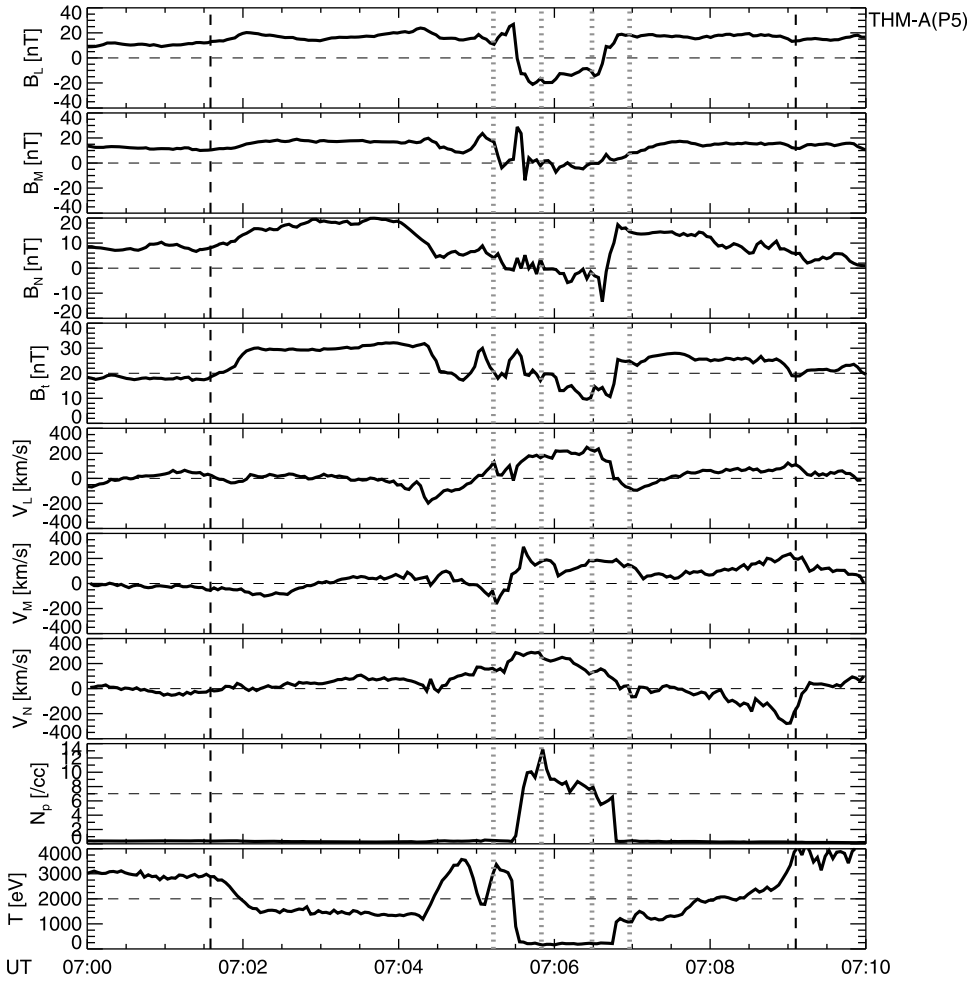

Figure 5. A zoom-in plot of the THEMIS-A's magnetic field and plasma data in LMN coordinates, which are transformed from GSM based on the MVA, during 10 min interval between 07:00 UT and 07:10 UT, is presented. From top to bottom, the plots show the three components of the magnetic field in LMN coordinates, the magnetic field intensity, the three components of the plasma velocity in LMN coordinates, the plasma number density and temperature, respectively. The time interval for the abrupt and transient magnetic field and plasma variations is indicated by two black broken lines. The durations for the THEMIS-A's magnetopause crossings are bracketed by two gray dotted lines.

10 min interval between 07:00 UT and 07:10 UT. In this plot, the matrix to transform the coordinates from GSM to LMN was made based on the magnetic field data during the first THEMIS-A magnetopause crossing interval between 07:05:13 UT and 07:05:50 UT. From top to bottom, the plots show the three components of the magnetic field in LMN coordinates, the magnetic field intensity, the three components of the plasma velocity in LMN coordinates, the plasma number density and temperature, respectively.

[36] During the time interval of the abrupt and transient variations as indicated by two black broken lines, the two sharp magnetic field polarity changes from +20 nT to −20 nT, and from −10 nT to +20 nT were observed in the B_L component as bracketed by two gray dotted lines, respectively. The first positive-to-negative B_L change from 07:05:13 UT to 07:05:50 UT is typical magnetic signature for the probe's outbound magnetopause crossing. The normal vector of the magnetopause surface, and the angles between the normal vectors on the GSM-XY and -XZ planes (N_{xy}, N_{xz}) and the GSM-XZ axes, are listed in Table 2. The normal vector of the magnetopause surface oriented to the tailward with slight duskward and southward inclinations in GSM-XY and -XZ planes. Therefore, the magnetopause surface was moving to the tailward and inward (toward the magnetosphere) directions, and quasi-perpendicularly encountered THEMIS-A. Associated prominent enhancements were observed in the B_M component and magnetic field intensity. Simultaneous V_L and V_N components showed the gradual enhancements, but clear "bipolar-type" perturbation with the positive followed by negative was found in the V_M component. This velocity "bipolar-type" signature strongly supports that the waves were generated on the tail-flank magnetopause [e.g., *Sibeck*, 1992; *Sibeck and Smith*, 1992]. The abrupt enhancement and decrease were observed in the plasma density (from 0.5/cc to 13.0/cc), and temperature (from 3400 eV to 200 eV) associated with the magnetopause surface waves.

Table 2. Normal Vectors of the Magnetopause Surface and the Angles Between the Normal Vectors on GSM-XY and -XZ Planes and GSM-XZ Axes

	(N_x, N_y, N_z)	θ_{Nxy} (deg)	θ_{Nxz} (deg)
First magnetopause crossing (07:05:32 UT)	(−0.9444, 0.0890, −0.3166)	174.62	−108.54
Second magnetopause crossing (07:06:43 UT)	(−0.2033, −0.9484, −0.2433)	−102.10	39.89

[37] The second negative-to-positive B_L discontinuity during the 29 s interval between 07:06:29 UT and 07:06:58 UT is associated with the probe's inbound magnetopause crossing. The vector of the normal to the magnetopause surface and the angles between the normal vectors on the GSM-XY and -XZ planes (N_{xy}, N_{xz}) and the GSM-XZ axes are also listed in Table 2. The normal vector of the magnetopause surface oriented to the outward (toward the magnetosheath) direction, and had the northward inclination in GSM-XZ plane. The direction of this magnetopause motion was outward, consistent with the THEMIS-A's inbound magnetopause crossing. During this magnetopause encounter, the negative-to-positive bipolar perturbation (from −14 nT to +18 nT) was found in the B_N component, and associated B_t presented the abrupt enhancement from 10 nT to 24 nT. Simultaneous B_M component did not show the striking fluctuation. No bipolar type perturbations were observed in the plasma velocity components as seen at the first magnetopause crossing. Gradual decrease of the velocity was seen in the V_L and V_N components, but the V_M component did not show the variations. The abrupt density decrease from 7.0/cc and 0.5/cc and temperature enhancement from 250 eV to 1500 eV were observed during this time interval.

[38] From the MVA, the orientation of the magnetopause surface normal has dramatically changed from inward to outward during 1.5 min. Furthermore, the bipolar-type perturbations were observed in the plasma velocity, and the abrupt decrease/enhancement of the plasma density and temperature were simultaneously found. These results obviously suggest that the magnetopause had the wavy structure. Therefore, THEMIS-A and -C, which were located at both sites of the tail-flank magnetopause, had detected highly magnetic field and plasma fluctuations due to the surface waves. In particular, THEMIS-A would instantaneously observe the magnetosheath plasma through these magnetopause surface waves.

6. THEMIS-D/-E and Simultaneous Cluster Duskside Magnetotail Observations From 07:05:48 UT to 07:13:19 UT

[39] The summary plots of the magnetic field and plasma data obtained from the THEMIS-D/-E probes, and the magnetic field data from Cluster, are exhibited in Figure 6. The presented time interval is the same as that in Figure 4. From top to bottom, the plots present the three components of the magnetic field in GSM coordinates and the magnetic field intensity from THEMIS-D (magenta) and -E (green), the three components of the magnetic field in GSM coordinates and the magnetic field intensity from Cluster-C2 (Salsa: green), -C3 (Samba: blue) and -C4 (Tango: red), the three components of the plasma velocity in GSM coordinates, the plasma number density and temperature from THEMIS-D/-E, respectively. Unfortunately, the magnetic field data from the Cluster-C1 (Rumba) and the plasma moment data from all Cluster's probes were not available during this time interval. Note that there was about 4 min time delay between the abrupt and transient magnetic field and plasma variations observed by THEMIS-A and THEMIS-D/-E, and the duration for these variations was 1 min shorter than that of THEMIS-A. Simultaneous Cluster satellite, whereas, stayed and observed in the duskside near-Earth magnetotail where it was just opposite to the THEMIS's dawnside observational location.

[40] The amplitudes for the abrupt and transient magnetic field variations observed by THEMIS-D/-E as bracketed by two black broken lines were much smaller than those by THEMIS-A. Furthermore, during the time interval when the abrupt and transient magnetic field and plasma were fluctuating, the background magnetic field values in the B_y, B_z components and B_t had been gradually enhanced. The δB_y, δB_z and δB_t, which are the values of the enhanced magnetic field, were 6.0 nT or 8.0 nT (not shown here). These slight background magnetic field enhancements were not seen in THEMIS-A's observation.

[41] Simultaneous magnetic field variations in the duskside near-Earth magnetotail were examined based on 4 s time resolution magnetic field data obtained from the three Cluster probes. However, there were no particular field fluctuations associated with the abrupt and transient magnetic field and plasma variations by THEMIS. We also examined the magnetic field fluctuations calculated by subtracting the average magnetic field values over the whole time interval from the observed magnetic field values, but they were so small, ranging between −1.0 nT and +1.0 nT (not shown here). Interestingly, in the duskside magnetotail, Cluster did not observe the abrupt and transient magnetic field fluctuations in all magnetic field components and the magnetic field intensity as THEMIS saw in the dawnside magnetotail. From the difference of the aspects for the magnetic field variations between the dawnside and duskside magnetotail, the abrupt and transient magnetic field and plasma variations would be local phenomena, that is, the phenomena occurring only in the dawnside magnetotail. Furthermore, the plausible physical mechanism to cause these characteristic magnetic field and plasma variations would be localized.

[42] The background values for all components of the plasma velocity of THEMIS-D/-E were almost 0 km/s over this time interval, and did not enhance even during the perturbed intervals as seen in the magnetic field. The amplitudes for the variations in all components of the plasma velocity were also smaller than those observed by THEMIS-A.

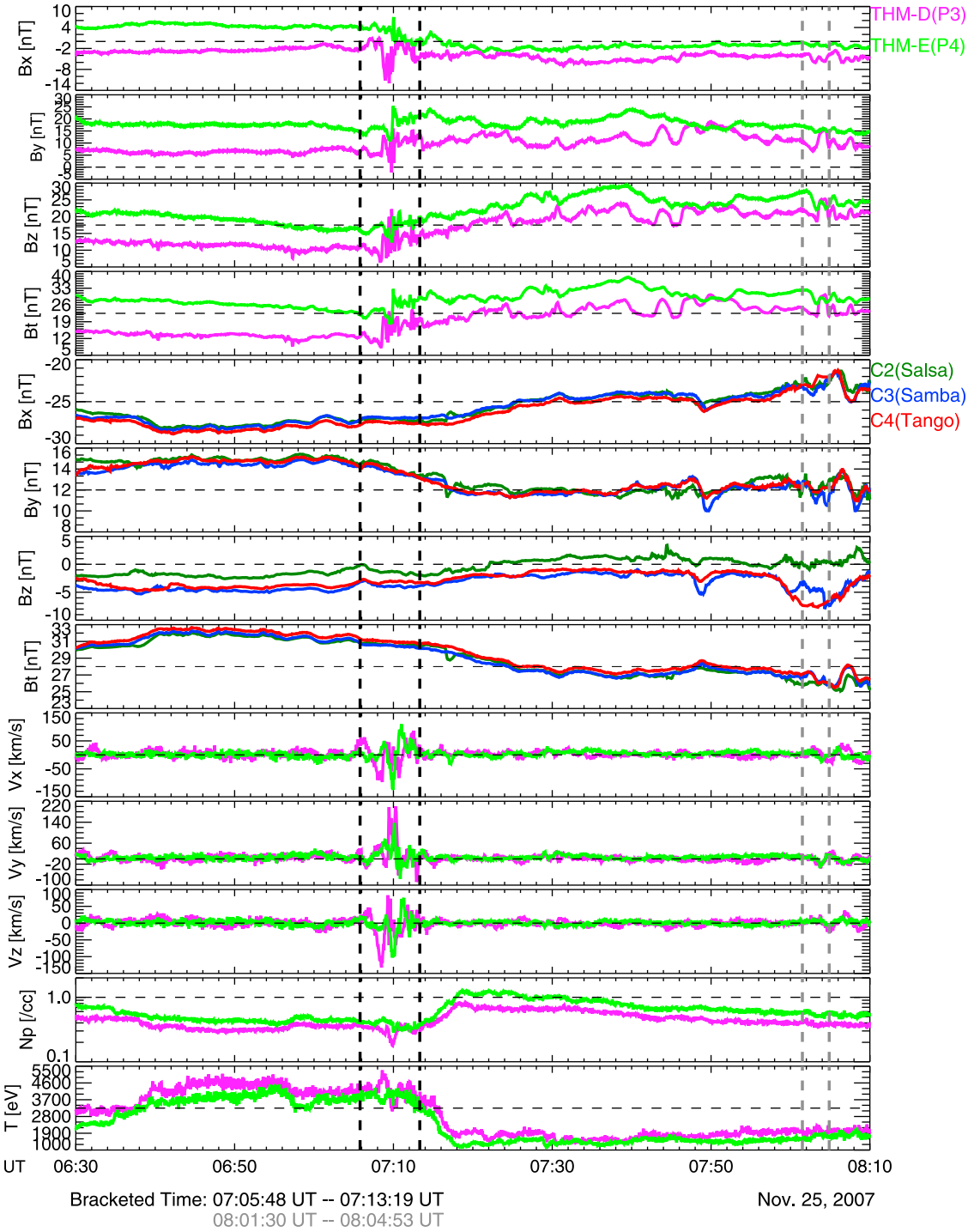

Figure 6. Plots of the magnetic field and plasma data obtained from THEMIS-D/-E, and the magnetic field data from Cluster, are shown. The presented time interval is the same as that in Figure 4. From top to bottom, the plots show three components of the magnetic field in the GSM coordinates and the magnetic field intensity from THEMIS-D (magenta) and -E (green), the three components of the magnetic field in the GSM coordinates and the magnetic field intensity from Cluster-C2 (Salsa: green),-C3 (Samba: blue) and -C4 (Tango: red), the three components of the plasma velocity in GSM coordinates, the plasma number density and temperature from THEMIS-D/-E, respectively. The magnetic field data from the Cluster-C1 (Rumba) and the plasma moment data from all Cluster's probes were not available during this time interval.

Interestingly, the patterns of the flow velocity variations were totally different from between THEMIS-D/-E, although these two probes were located very close to each other. All velocity components observed by THEMIS-E were perturbing as "bipolar-type," but the V_x and V_z components by THEMIS-D were fluctuating between −90 km/s and +90 km/s, and between −120 km/s and +90 km/s, respectively. Associated V_y component of THEMIS-D presented duskward plasma flow burst. In simultaneous plasma density, only a little negative impulse was found by THEMIS-D at around 7:10 UT, but particular density variations in association with the magnetic field and plasma velocity perturbations were not exhibited by THEMIS-D/-E. From 07:14 UT to 07:19 UT just after the magnetic field and plasma variations, the density began to enhance gradually from 0.4/cc to about 1.0/cc. The temperature measured by THEMIS-D/-E did not also show significant fluctuations during the time interval of the abrupt and transient magnetic field and plasma variations, although only THEMIS-D detected the small perturbations at around 07:09 UT. However, the abrupt decrease from 3400 eV to 1500 eV was detected by THEMIS-D/-E from 07:14 UT to 07:19 UT.

[43] During about 3.5 min interval from 08:01:30 UT to 08:04:53 UT as bracketed by two gray broken lines, THEMIS-A observed the second abrupt and transient magnetic field and plasma variations. However, associated striking variations were not detected by THEMIS-D/-E and Cluster in both the magnetic field and plasma parameters.

[44] From this observational discrepancy between THEMIS-A and THEMIS-D/-E, the abrupt and transient magnetic field and plasma variations observed by THEMIS-A and THEMIS-D/-E would have different physical mechanisms.

7. Geomagnetic Field Variations: Ground-Based Observation

[45] The abrupt and transient magnetic field and plasma variations were observed clearly in the dawnside near-earth magnetotail, but not in the duskside magnetotail. To pursue the reason of such unique phenomena, we need to know what happened in the inner-magnetosphere by obtaining information on the geomagnetic field during that time period. We then examined the detailed geomagnetic field variations using the magnetic field data with 1 s time resolution taken from high-latitude Canadian magnetometer chain (Canadian Array for Realtime Investigations of Magnetic Activity; CARISMA) [*Mann et al.*, 2008]. The orbit of THEMIS was just passing above the CARISMA magnetometer chain during focused magnetic field and plasma variations. Therefore, the magnetic field data from CARISMA are useful for investigating the geomagnetic disturbance during the THEMIS's observational interval.

[46] Figure 7a shows the locations of the eight CARISMA stations used in this study. Their geodetic latitude and longitude values (the values of "longitude - 360.0" are also shown since the range of the longitude is between −180 degrees and 180 degrees), and the universal time of local magnetic (LM) midnight at each station are listed in Table 3. Because the CARISMA magnetometer chain is located in the North America sector, the local magnetic midnight is time zone between about 6:20 UT and 8:00 UT.

[47] The geomagnetic field variations observed by the eight CARISMA stations and their corresponding variations of the $SYM - H$ index, which is 1 min average of the value of D_{st} index, are presented in Figure 7b. The eight CARISMA stations shown in Figure 7b and Table 3 have been sorted in decreasing order of latitude. In these plots, the fluctuation values for the north-southward (X-axis) magnetic field component, which are calculated by subtracting the average magnetic field values over the presented time interval from the observed magnetic field values, are plotted. The time intervals during which THEMIS-A (shown with green as labeled with "1") and THEMIS-D/-E (magenta as labeled with "2") observed the abrupt and transient magnetic field and plasma variations are bracketed by two gray broken lines. Note that the two time intervals are overlapped about 3 min. During the "1" and "2" time intervals, the sudden decrease, negative bay and periodic fluctuations (especially at GILL, ISLL, PINA and GULL stations) were clearly observed at all stations except the highest-latitude TALO station. However, just after the "1" and "2" time intervals, these geomagnetic variations were clearly observed also at TALO station. These observed variations are clear evidence that the inner magnetosphere and near-Earth magnetotail are disturbed (or start to be disturbed) by the phenomena, such as substorm due to an encounter of the IMF-B_x discontinuity with the magnetosphere. However, no striking variations were seen in associated $SYM - H$, indicating neither the plasma injection into the inner magnetosphere from the distant magnetotail nor the ring current development due to a magnetic storm during the "1" and "2" time intervals. Furthermore, the absence of the $SYM - H$ variations also means that the current disruption and the associated current to the ionosphere via the substorm current wedge did not occur during these time intervals. Because large (<−300 nT) and prolonged (over 1 h) negative bay variations and magnetic fluctuations were not observed at all stations during the whole time interval, the intensity (scale) of the phenomena plausibly induced by an encounter of the IMF-B_x discontinuity with the magnetosphere is not very strong.

[48] The geomagnetic field and $SYM - H$ variations during the second abrupt and transient magnetic field and plasma variations observed by THEMIS-A (bracketed by two green broken lines as labeled with "3"), whereas, were not found. The absence of the geomagnetic field variations indicates that the substorm and magnetic storm do not "directly" contribute to cause these second magnetospheric magnetic field and plasma variations.

[49] In section 8, we will report the relationship between the auroral brightening and associated geomagnetic activity. From this analysis, we will clarify whether the phenomena caused by an IMF-B_x discontinuity are "substorms."

8. Relationship Between the Auroral Brightening and Geomagnetic Activity

[50] During the THEMIS-A and THEMIS-D/-E observational intervals, the geomagnetic field observed at high-latitude ground observatories showed clear negative bay and periodic fluctuations. These characteristic geomagnetic field variations are clear evidence for an occurrence of a substorm in the near-Earth magnetotail. However, if a

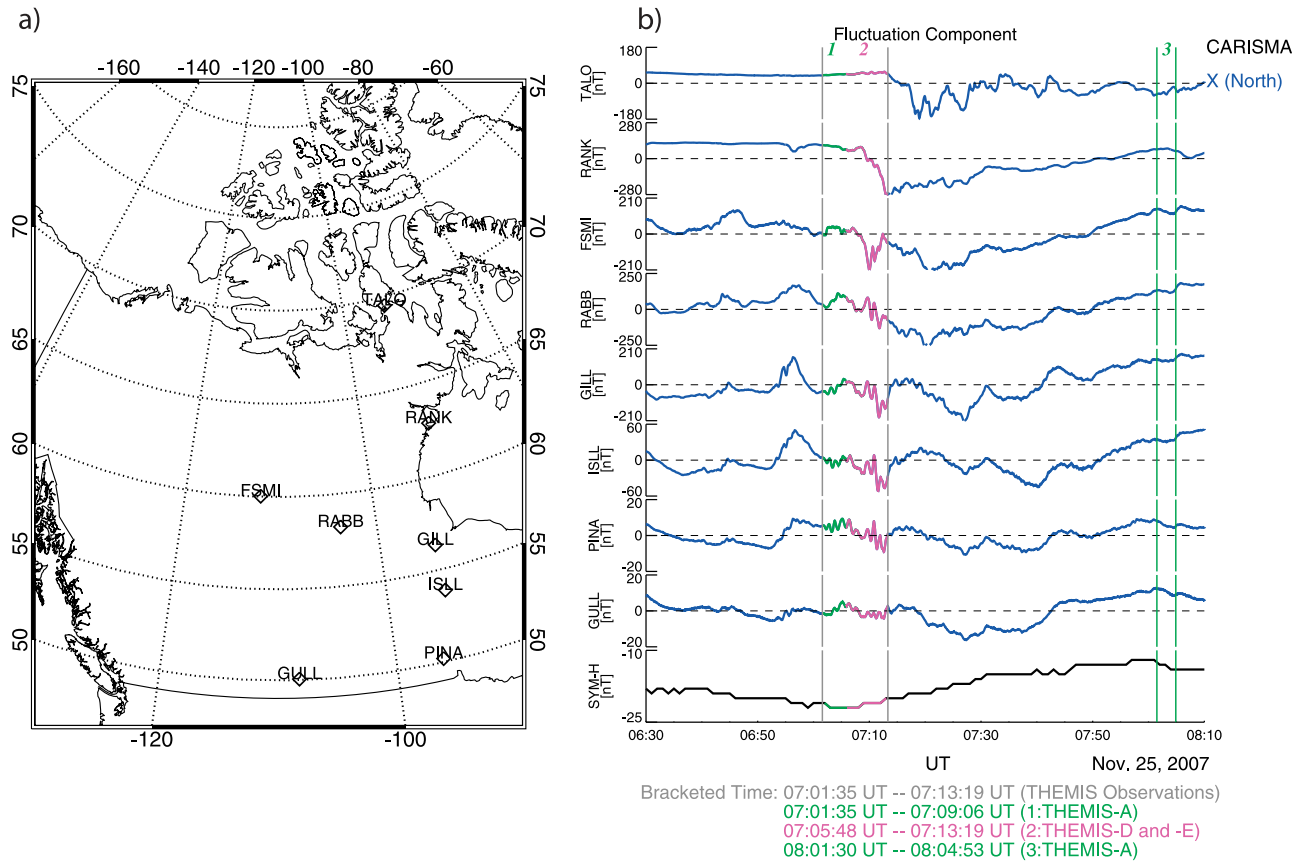

Figure 7. (a) The locations of the eight ground geomagnetic field observatories of CARISMA used in this study are shown. The geodetic latitude and longitude, and the universal time of the local magnetic (LM) midnight at each station, are listed in Table 3. (b) The variations in the north-southward (X-axis) magnetic field component observed by the eight CARISMA stations and their corresponding variations of the $SYM - H$ index, which is 1 min average of the value of D_{st} index, are presented, respectively. These eight CARISMA stations have been sorted in decreasing order of latitude. The time intervals during which THEMIS-A (shown with green as labeled with "1") and THEMIS-D/-E (magenta as labeled with"2") observed the abrupt and transient magnetic field and plasma variations are bracketed by two gray broken lines. The time interval corresponding to the second abrupt and transient magnetic field and plasma variations observed by THEMIS-A is bracketed by two green broken lines as labeled with "3."

substorm occurred, associated auroral activation should also be observed. We then examined the relationship between the auroral brightening and geomagnetic activity. Figure 8a shows the plots of the *AU*, *AL* and *AE* indices during 1 h and 40 min interval between 06:30 UT and 08:10 UT. The time intervals around the main phases for the abrupt and transient magnetospheric magnetic field/plasma variations observed by THEMIS-A and THEMIS-D/-E are shown with broken lines a–d and d–i, respectively. The red letters b and c and blue letters f, g, and h in Figure 8a denote "exact" main phase intervals for the abrupt and transient magnetic field/plasma variations, respectively.

[51] During the whole time interval, the geomagnetic condition had been active because all of the three indices had the tendency to enhance. These three indices were variable also during the interval of the abrupt and transient magnetic field and plasma variation. In particular, the *AU* index showed the abrupt enhancement, and two-stepwise impulsive enhancements were observed in simultaneous *AL* index. During the THEMIS-A's observational interval, the *AL* index abruptly enhanced from −240 nT to −300 nT, but the *AE* decreased from about 500 nT to 380 nT. Simultaneous *AU* index did not show the particular variation. The respective *AL*, *AU* and *AE* indices increased their values

Table 3. Geodetic Latitude and Longitude of the Eight CARISMA Magnetometer Stations and the Universal Time of the Local Magnetic (LM) Midnight at Each Station

Station (Code)	Latitude (deg)	Longitude (Longitude – 360.0) (deg)	LM Midnight (UT)
Taloyoak (TALO)	69.54	266.45 (−93.55)	06:37
Rankin Inlet (RANK)	62.82	267.89 (−92.11)	06:25
Fort Smith (FSMI)	60.03	248.07 (−111.93)	08:08
Rabbit Lake (RABB)	58.22	256.32 (−103.68)	07:27
Gillam (GILL)	56.38	265.36 (−94.64)	06:34
Island Lake (ISLL)	53.86	265.34 (−94.66)	06:36
Pinawa (PINA)	50.20	263.96 (−96.04)	06:39
Gull Lake (GULL)	50.06	251.74 (−108.26)	07:47

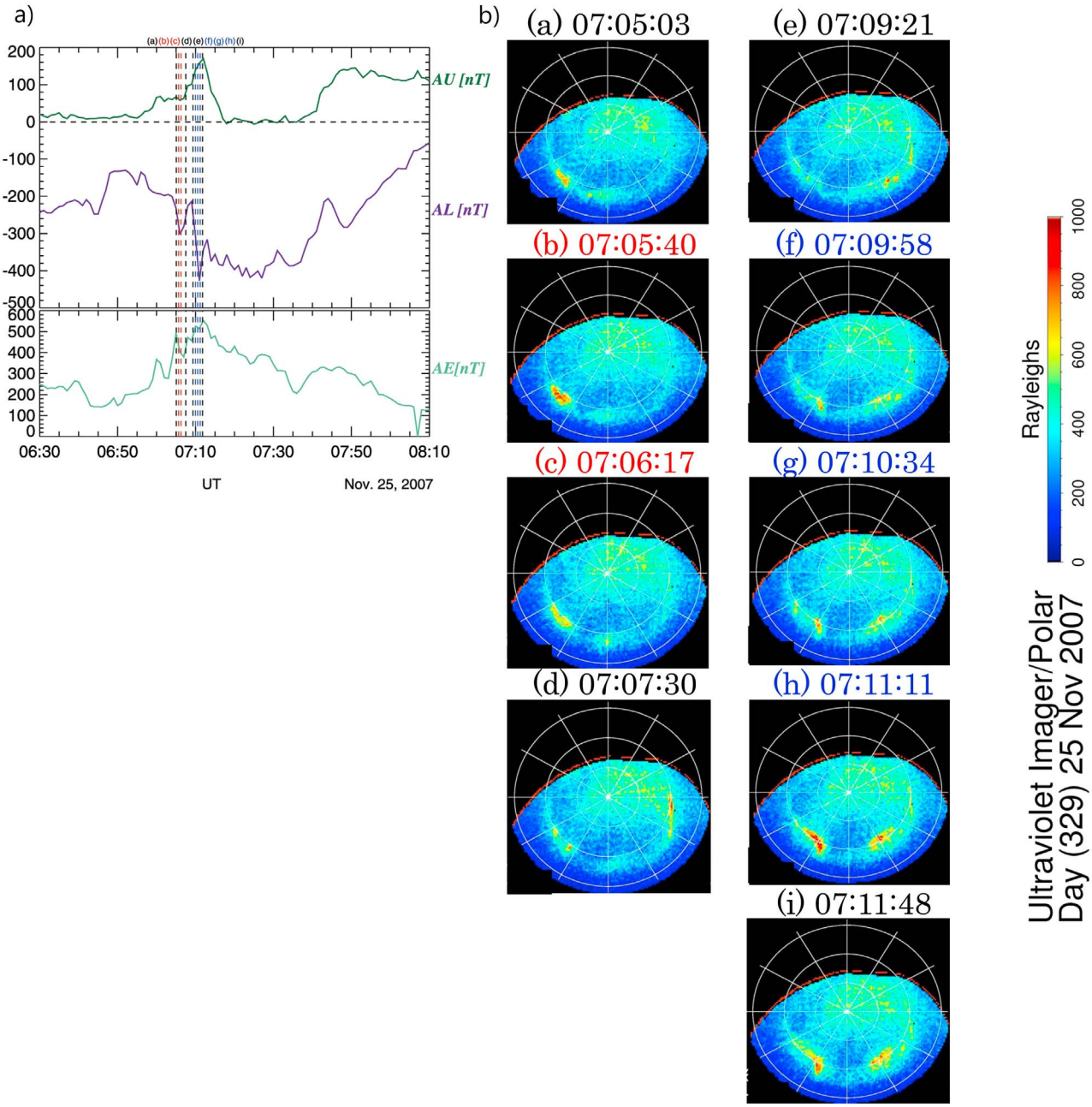

Figure 8. (a) Plots of the *AU*, *AL* and *AE* indices during 1 h and 40 min interval between 06:30 UT and 08:10 UT are presented. The time intervals around the main phases for the abrupt and transient magnetospheric magnetic field/plasma variations observed by THEMIS-A and THEMIS-D/-E are shown with the broken lines a–d and e–i, respectively. Red letters b and c and blue letters f, g, and h denote "exact" main phase intervals for the abrupt and transient magnetic field/plasma variations. (b) Shown are consecutive global auroral ultraviolet images obtained from Polar during THEMIS-A (images a–d) and THEMIS-D/-E (images e–i) observational intervals. The color code is assigned according to the intensity of the auroral brightness in units of Rayleigh. The top, left, bottom, and right sides of each plot present 12h, 18h, 0h and 6h MLT, respectively. The AACGM latitude contours are drawn every 10°.

from −240 nT to −420 nT, from 120 nT to 170 nT, and from 500 nT to 560 nT during the THEMIS-D/-E's observational interval. The enhancements for these three indices during the THEMIS-D/-E's time interval were much more striking than those during the THEMIS-A's interval. This result suggests that the disturbance in the near-Earth magnetotail during the THEMIS-D/-E's time interval is larger than that during the THEMIS-A's interval. Therefore, some signatures for the phenomena as disturbing the near-Earth magnetotail should also be observed by THEMIS-D/-E.

[52] Associated global auroral activity was also examined based on the Ultraviolet Imager (UVI) instrument on board

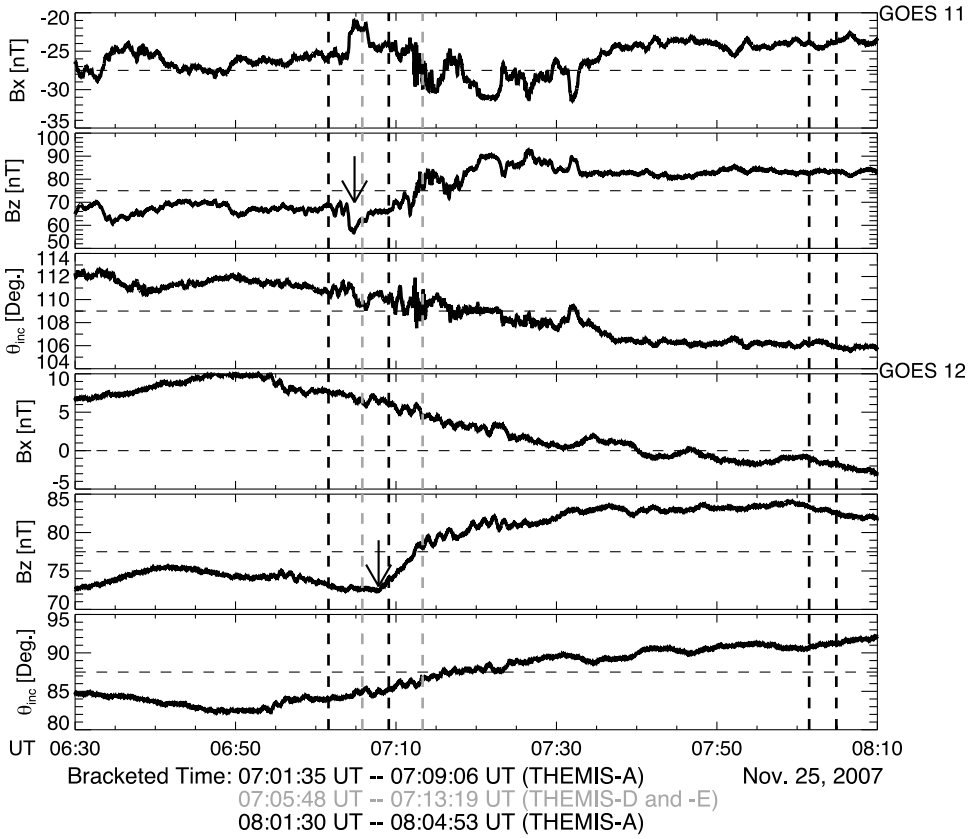

Figure 9. Plots of the magnetic field data with 0.5 s high-time resolution obtained from the GOES-11 and -12 geosynchronous satellites during 1 h and 40 min interval from 06:30 UT to 08:10 UT are presented. From top to bottom, the plots show the GSM-X and -Z components of the magnetic field measured by GOES-11, their inclination angle between the B_x and B_z components (θ_{inc}), the B_x and B_z components in GSM coordinate system from GOES-12 and their inclination angle, respectively. The THEMIS-A and THEMIS-D/-E's observational intervals are bracketed by two black and gray broken lines, respectively.

the Polar satellite. Figure 8b shows the consecutive auroral imagers corresponding to the observational intervals of THEMIS-A (images a–d) and THEMIS-D/-E (images e–i). Particular time intervals in red and blue numerals are corresponding to "exact" main phases for the abrupt and transient magnetic field/plasma variations observed by THEMIS-A and THEMIS-D/-E. Here we used the Lyman-Birge-Hopfield long (LBHL) band having its wavelength of ~170.0 nm with 36 s exposure time (see *Torr et al.* [1995] for details). The color code is assigned according to the intensity of the auroral brightness in units of Rayleigh. Furthermore, the Altitude Adjusted Corrected Geomagnetic Model (AACGM) [*Baker and Wing*, 1989] was used to calculate the MLT and magnetic latitude (MLAT) for these auroral images. The top, left, bottom and right sides of each image show 1200, 1800, 0000, and 0600 MLT, respectively. The contours of AACGM latitude are drawn every 10 degrees.

[53] During the THEMIS-A observational interval, the whole auroral activity was quiet. One small and weak auroral brightening spot was clearly found around 68 degrees MLAT whose MLT range was between 2000 h and 2200 h at the times of Figure 8b, images b and c. The auroral activity had been quiet also during the THEMIS-D/-E observational interval. However, in the main phase for the magnetospheric magnetic field/plasma variations (particularly, at time of image h), two small and weak auroral spots were observed at about 70 degrees MLAT whose MLT was around 2200 h and 0200 h.

[54] From these results, the global auroral activity associated with the phenomena due to an IMF-B_x discontinuity little occurred, even though the geomagnetic field was fairly disturbed. Therefore, "pure" substorm was not, but "substorm-like" phenomena were triggered by an encounter of the IMF-B_x with the magnetosphere.

[55] In section 9, we examine detailed magnetic field variations at geosynchronous altitudes, in order to clarify further relationship between the abrupt and transient magnetospheric magnetic field/plasma variations and the substorm-like phenomena.

9. Magnetic Field Variations at Geosynchronous Orbit: GOES-11 and -12 Observations

[56] We investigated the magnetic field variations at the geosynchronous orbit during the same time intervals of THEMIS, Cluster and ground-based observations, to clarify more whether the abrupt and transient magnetic field and plasma variations were related with the substorm-like phenomena. Figure 9 presents the plots of the magnetic field data with 0.5 s high-time resolution obtained from GOES-11

and -12 during 1 h and 40 min interval from 06:30 UT to 08:10 UT. From top to bottom, the plots show the X and Z components of the magnetic field in GSM coordinates measured by GOES-11, their inclination angle between the B_x and B_z components (θ_{inc}) calculated with $\tan^{-1}\left(\frac{B_z}{B_x}\right)$, the B_x and B_z components in GSM coordinate system from GOES-12, and their inclination angle, respectively. The THEMIS-A and THEMIS-D/-E's observational intervals are bracketed by two black and gray broken lines, respectively.

[57] The B_x component observed by GOES-11 slightly decreased its value (about 8 nT) during the first THEMIS-A observational interval. However, it had enhanced tailward from around 07:05:48 UT, which was the start time of the THEMIS-D/-E's observation, to 07:15 UT beyond the observational interval of THEMIS-D/-E. Although the B_x component had been variable during about 20 min between 7:15 UT and 7:33 UT, it had been stable after 7:33 UT. The B_x enhancement and decrease are corresponding to the tailward stretching of the magnetic field lines caused by the enhanced tail current and the tail dipolarizations, respectively. These magnetic field line configuration changes in the inner magnetosphere are seen also at "pure" substorm process. Simultaneous B_z component started to enhance gradually from 07:03:30 UT within the first THEMIS-A's interval as shown with an arrow, to around 07:23 UT, although some perturbations were in the main enhancement trend of the B_z component. This B_z gradual enhancement is also typical signature of the dipolarization. From 07:23 UT to 07:33 UT, the B_z component showed small fluctuations, but had been stable after 07:33 UT as well as the B_x component. The gradual decrease of the inclination angle during the whole interval (in particular, from 07:01:35 UT to around 07:37 UT) is most likely due to GOES-11 moving to the other location (it moved roughly two MLT sectors). Furthermore, this angle decrease clearly suggests that the magnetic field lines had been stretched into the tailward direction. Therefore, the variations of both the B_x and B_z components, and associated gradual inclination angle decrease evidently show the tail dipolarizations due to the substorm-like phenomena.

[58] The B_x component observed by GOES-12 had been decreased from 06:30 UT to about 07:30 UT, but began to enhance with the polarity change from 07:45 UT to 08:10 UT. During the first THEMIS-A and THEMIS-D/-E time intervals, the B_x component had decreased, and the small wavy perturbations were found in the main trend. These wavy magnetic field oscillations were observed also at the ground magnetic observatories because GOES-12 and CARISMA magnetometer chain were roughly in the same pre-midnight (22 h $\sim$ 23 h MLT) sector. Simultaneous B_z component began to enhance from 07:07:35 UT as shown with an arrow. Note that there was 4 min time delay for the start time of the B_z enhancement between GOES-11 and -12. The small wavy perturbations were also observed in the main trend of the B_z component as well as the B_x component and the magnetic field observed at the ground-magnetic observatories. In both the B_x and B_z components, these small wavy magnetic perturbations had been seen from 06:55 UT to 07:25 UT. The inclination angle had been increased gradually during the whole time interval, indicating that the orientation of the magnetic field line closed to the northward in association with the dipolarization. This gradual inclination angle enhancement, of course, shows that GOES-12 also moved to the other location within about 2 MLT sectors. The gradual B_x decrease, and the enhancements of both the B_z component and magnetic inclination angle strongly suggest that GOES-12 also detected the magnetic signature of the tail dipolarizations as well as GOES-11. Accordingly, this observed dipolarization was a large-scale phenomenon covering over at least 2 MLT sectors.

[59] During the second interval of the THEMIS-A's observation, the magnetic field enhancement and decrease were not found by both GOES-11 and -12. The particular change for simultaneous inclination angle was not also seen. This result shows that the substorm-like phenomena did not directly contribute to the second abrupt and transient magnetic field and plasma variations observed by THEMIS-A.

[60] As a double check, simultaneous data of the time variation of the plasma energy (E-t diagram) at geosynchronous orbit, observed by the satellites of Los Alamos National Laboratory (LANL), were also examined. However, striking injection of high-energy ion and electron from the magnetotail into the geosynchronous altitudes, associated with a magnetic storm and intense substorm(-like phenomena), was not observed (not shown here). This result is consistent with no particular $SYM - H$ variations as pointed out in section 8.

10. Magnetic Field Fluctuations Associated With the Substorm-Like Phenomena

[61] An encounter of the IMF-B_x discontinuity with the magnetosphere evidently plays a crucial role for triggering the substorm-like phenomena. Resultant abrupt and transient magnetic field and plasma variations were observed by THEMIS-D/-E. From the magnetic field observations with both the ground magnetic observatories and geosynchronous satellites, significant magnetic field fluctuations were found around the time intervals of the THEMIS-D/-E observations. We then investigated whether these magnetic field perturbations were observed in association with the substorm-like phenomena, and how the relationship between the abrupt and transient magnetic field/plasma variations and the substorm-like phenomena is.

[62] Figure 10a shows the summary plot of the fluctuations for the B_z components measured by THEMIS-A, THEMIS-D/-E, the three Cluster probes, GOES-11, -12 and the north–south magnetic field component (B_x) at the Gillam station. This ground observatory was the closest to the foot point during which the abrupt and transient variations were observed by THEMIS-A and THEMIS-D/-E. The foot point of THEMIS mapped along field lines was calculated using Tsyganenko 96 model [*Tsyganenko*, 1995] inputted with the parameter values of the IMF-B_y (1.40 nT), IMF-B_z (-1.15 nT), P_d (1.6 nPa) and D_{st} index (-27 nT). The plot interval is 30 min between 06:55 UT and 07:25 UT. The time intervals during the THEMIS-A and THEMIS-D/-E observations are bracketed by two cyan and red broken lines, respectively.

[63] During the time interval that THEMIS-A observed the abrupt and transient magnetic disturbance, associated large-amplitude magnetic fluctuations and particular wave structures were not found in the B_z components by the three Cluster probes. However, in the geosynchronous altitudes,

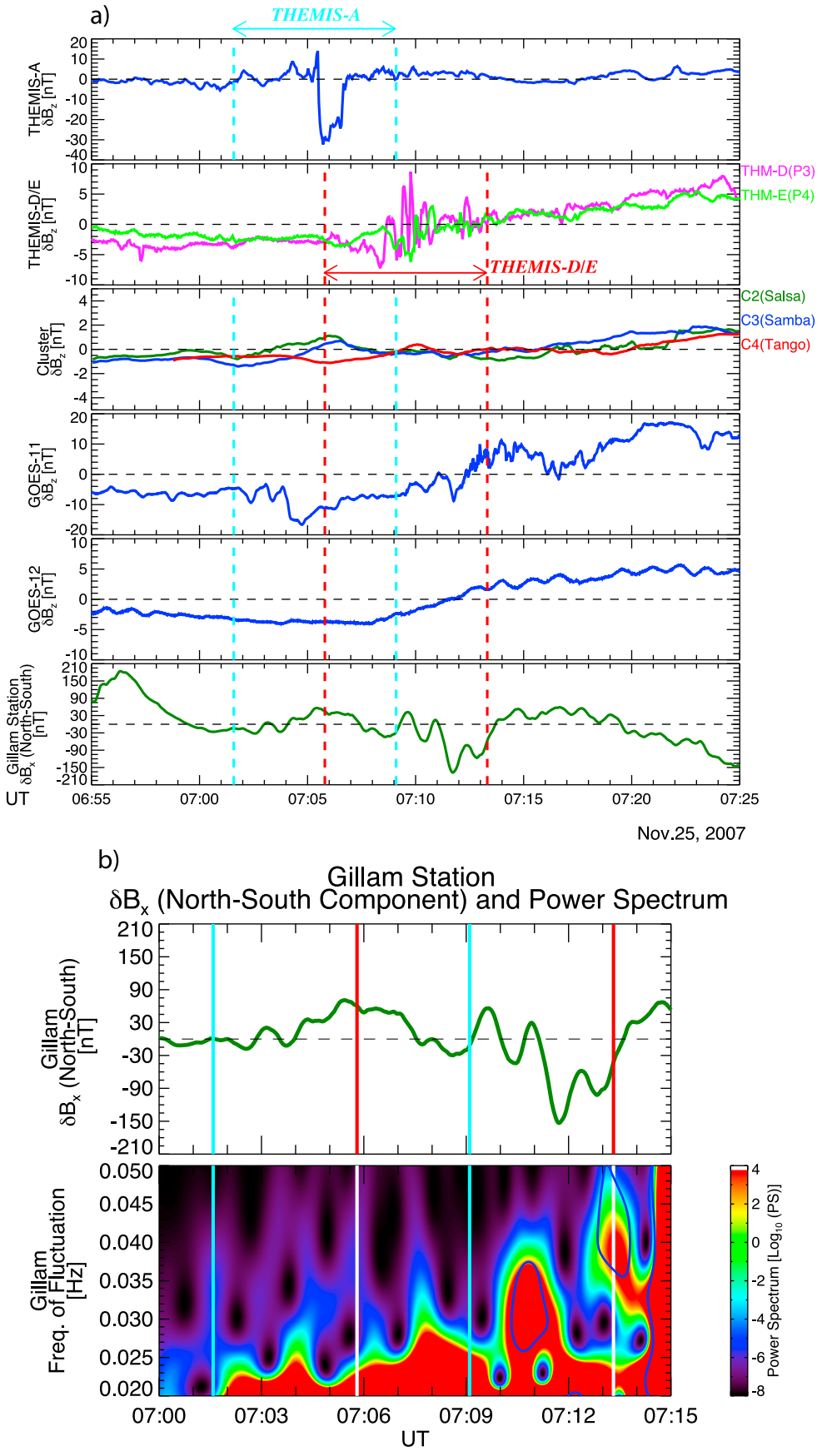
a)
THEMIS-A
THEMIS-A δBz [nT]
THEMIS-D/E δBz [nT]
THM-D(P3)
THM-E(P4)
THEMIS-D/E
Cluster δBz [nT]
C2(Salsa)
C3(Samba)
C4(Tango)
GOES-11 δBz [nT]
GOES-12 δBz [nT]
Gillam Station δBx (North-South) [nT]
UT
06:55
07:00
07:05
07:10
07:15
07:20
07:25
Nov.25, 2007
b)
Gillam Station
δBx (North-South Component) and Power Spectrum
Gillam δBx (North-South) [nT]
Gillam Freq. of Fluctuation [Hz]
Power Spectrum [Log10 (PS)]
07:00
07:03
07:06
07:09
07:12
07:15
UT

Figure 10

the B_z components by GOES-11 and -12 have just started to enhance, suggesting the dipolarization for the substorm-like signature was occurring. Furthermore, some small periodic perturbations between 07:07 UT and 07:10 UT were seen. The B_x component at the ground station was also periodically fluctuating from 07:02 UT to 07:06 UT. While the B_z component by THEMIS-D/-E showed the transient disturbance, the B_z components of the three Cluster probes did not show associated fluctuations and waves as well as the THEMIS-A's interval. Simultaneous GOES-11 and -12 observed the gradual B_z enhancement associated with the substorm-like phenomena. In particular, the fluctuations with larger amplitudes than those seen during the THEMIS-A's interval were shown in the B_z enhancement observed by GOES-11. The clear wave structures from about 07:09 UT to 07:13 UT were found in the B_x component observed at the ground observatory. The wavy magnetic field variations were clearly observed by both GOES and the ground magnetic observatory also after the time interval when the abrupt and transient magnetic field and plasma variations were seen.

[64] Comparing the inner magnetospheric magnetic field fluctuations during the THEMIS-A's observational interval with those during the THEMIS-D/-E interval, the magnetic disturbances associated with the substorm-like phenomena were obviously seen during the THEMIS-D/-E's observational interval. This result strongly supports that the abrupt and transient magnetic field/plasma variations observed by THEMIS-D/-E were caused by the substorm-like phenomena. During the THEMIS-A's interval, the magnetopause surface waves were generated by KHI. Therefore, associated inner magnetospheric magnetic perturbations should be smaller than the magnetic field fluctuations observed during the THEMIS-D/-E interval.

[65] Based on the aspect for the magnetic field fluctuations observed by GOES and ground magnetic observatory, the waves with the very long wavelengths would be launched in association with the substorm-like phenomena. Although the abrupt and transient magnetic field variations observed by THEMIS did not contain clear wave structures, GOES and ground magnetic observatory clearly detected associated waves, which were seen also after the THEMIS's observational intervals. Furthermore, Cluster did not observe any wave signature in the magnetic field due to moving significantly to another location over the duration of associated waves.

[66] Next, we examined whether the waves seen during the THEMIS observational intervals are associated with the substorm-like phenomena. If the dominant frequency range for the observed waves was consistent with the Pi2 wave range between 6.7 mHz and 25.0 mHz, it was strongly supported that the substorm-like phenomena were exactly occurring in the near-Earth magnetotail. This is because the Pi2 waves are a sensitive indicator of substorm(-like phenomena)'s occurrence [e.g., *Saito et al.*, 1976]. Figure 10b shows the magnetic field fluctuations of the B_x component observed at the Gillam station, and associated wave power spectrum calculated by wavelet analysis using Morlet function as the mother wavelet function [*Torrence and Compo*, 1998] during 15 min between 07:00 UT and 07:15 UT. The vertical axis of the bottom plot gives the frequency of the magnetic field fluctuation, and the color code is assigned according to the logarithmic values of the intensity of the wave power spectrum. The significance level higher than 93% for the power spectrum intensity is surrounded by blue solid lines. The time intervals when THEMIS-A and THEMIS-D/-E observed the abrupt and transient magnetic field and plasma variations are bracketed by solid cyan and red (white) solid lines, respectively. The power spectrum intensity lower than 25.0 mHz had been high during the THEMIS's observational time interval. In particular, the significant high levels for the wave power spectrum intensity were marked over the ranges between 25.5 mHz and 37.5 mHz during the THEMIS-D/-E observational interval. These frequency ranges, showing the high spectrum intensity for the observed waves, were almost consistent with that of the Pi2 waves. This result clearly suggests that the waves associated with the substorm-like phenomena were those with the Pi2 range.

11. Discussion

11.1. On the Interaction Between the Magnetosphere and IMF-B_x Discontinuity

[67] We examined the responses for the magnetic field and plasma in the dawnside near-Earth magnetotail due to an encounter of a positive-to-negative IMF-B_x discontinuity. The particular enhancement of the solar wind ram (dynamic) pressure and southward IMF-B_z structure was not associated with this discontinuity. Furthermore, this magnetic discontinuity must be a HCS, separating two high-speed solar wind streams with different velocity and magnetic polarity. During the time intervals that THEMIS observed the abrupt and transient magnetospheric magnetic field and plasma variations, Pi2 waves, the magnetic field enhancement associated with the dipolarization, and stretching of the magnetic field lines were observed in the inner magnetosphere. However, associated auroral activity was quiet. From these results, not "pure" substorm but "substorm-like" phenomena occurred in the near-Earth magnetotail due to an encounter of the IMF-B_x discontinuity.

Figure 10. (a) The summary plots of the fluctuations for the B_z components obtained from THEMIS-A, THEMIS-D/-E, the three Cluster probes, GOES-11 and -12, and the north–south magnetic field component (B_x) at the Gillam station closest to the foot point during the THEMIS-A and THEMIS-D/-E observational intervals are presented, respectively. The plot interval is 30 min between 06:55 UT and 07:25 UT. The time intervals during the THEMIS-A and THEMIS-D/-E observations are bracketed by two cyan and red broken lines, respectively. (b) The magnetic field fluctuations of the B_x component observed at the Gillam station, and associated wave power spectrum calculated by wavelet analysis using Morlet function as the mother wavelet function [*Torrence and Compo*, 1998], are respectively shown during 15 min between 07:00 UT and 07:15 UT. Vertical axis of the bottom plot gives the frequency of the magnetic field fluctuation, and the color code is assigned according to the logarithmic values of the intensity of the wave power spectrum. The significance level higher than 93% for the power spectrum intensity is surrounded by blue solid lines. The THEMIS-A and THEMIS-D/-E observational intervals are bracketed by solid cyan and red (white) solid lines, respectively.

[68] In order to elucidate the physical link between an encounter of the IMF-B_x discontinuity with the magnetosphere and observed moderate substorm-like phenomena, it is necessary to consider how the substorm-like phenomena occurred. The magnetic reconnection process at the magnetotail lobe region is the most plausible mechanism to cause the substorm-like phenomena. In the case that IMF has the dominant sun-earthward magnetic structure, magnetic reconnection might occur at the magnetotail lobe regions in the Northern and Southern hemispheres as mentioned by *Sibeck et al.* [1985] and *Gosling et al.* [1986].

[69] Before a passage of the discontinuity, the IMF-B_x had been positive for about 30 min. During this interval, the magnetic reconnection is expected to occur at the magnetotail lobe region in the Southern Hemisphere where the B_x component of the internal magnetic field is always negative. After a discontinuity encounter, the IMF-B_x suddenly changed its orientation from positive to negative, and possible location of the magnetic reconnection would suddenly switch from the Southern Hemisphere to the Northern Hemisphere where the internal B_x component is always positive. This sudden change for the location of magnetic reconnection could release the magnetic energy which had been deposited during the positive IMF-B_x interval, to trigger the substorm-like phenomena. However, we do not obtain clear evidence for an occurrence of the magnetotail lobe reconnection. Therefore, we cannot elucidate the detailed triggering mechanism for moderate substorm-like phenomena under this specific solar wind condition in this study.

11.2. Magnetospheric Responses to a Discontinuity's Passage

[70] When the IMF-B_x discontinuity encountered the magnetosphere, Pi2 waves associated with the substorm-like phenomena were observed by both GOES and the ground magnetic observatories as located in the same MLT sector. Furthermore, GOES and the ground station detected respective B_z enhancements and B_x negative bay variations as typical magnetic variations of tail dipolarizations. These waves and magnetic field variations are direct evidence that the substorm process is triggered by an encounter of the IMF-B_x discontinuity with the magnetosphere. However, the triggered process is not "pure" substorm because associated striking global auroral activation was absent.

11.2.1. Dawnside Tail-Flank Magnetopause Responses

[71] THEMIS-A and -C experienced the intermittent and multiple magnetopause crossings caused by surface waves. THEMIS-A observed resultant abrupt and transient magnetic field and plasma variations due to instantaneously seeing the magnetosheath plasma. To check whether THEMIS-A actually saw the transient magnetosheath plasma, we compared the number density values at the main phases of the two impulsive variations observed by THEMIS-A with those in the solar wind measured by ACE and Geotail. The density in the magnetosphere (about 16.5/cc and 13.0/cc) was roughly 4 times as much as that in the solar wind (about 3.0/cc $\sim$ 4.0/cc). The compression ratio of the solar wind density between before and after a passage of bow shock is typically around 4 [e.g., *Spreiter et al.*, 1966]. Therefore, the impulsive density variations are attributed to the THEMIS-A's detection of the magnetosheath (shocked solar wind) plasma. A possible physical interpretation for the THEMIS-A's transient magnetosheath plasma detection could be done because the IMF-B_x discontinuity shifted the magnetopause inward closer to the THEMIS-A's location.

[72] Kelvin-Helmholtz instability (KHI) is widely considered to be candidate of the mechanism to generate the waves on the magnetopause surface. The drastic changes, such as the solar wind dynamic pressure, were not seen except for a B_x discontinuity. Only a velocity shear between in the solar wind and the magnetosphere sites is required to generate KHI. In this case, high-speed streams with the velocity of about 600 km/s were clearly observed in the solar wind, and the plasma velocity in the magnetospheric side was much slower (about 50 km/s). *Pu and Kivelson* [1983a] demonstrated the relationship between the growth rate of KHI in the nightside magnetopause and the solar wind velocity normalized by the Alfvén velocity in the magnetosphere (see *Pu and Kivelson* [1983a, Figure 8] and also *Pu and Kivelson* [1983b]). This relation was obtained under an assumption that the normalized solar wind velocity is parallel to both IMF and the magnetospheric magnetic field line. Using the ratios of the magnetic field ($B_{msph}/B_{sw} \sim 10.0$), number density ($N_{sw}/N_{msph} \sim 22.6$) and velocity ($V_{sw}/V_{msph} \sim 12.0$) between the magnetospheric (msph) and solar wind (sw) sites in our case, and further assuming that KHI waves dominantly propagate to the field-aligned direction, we checked roughly the growth rate of KHI for the normalized solar wind velocity. As a result, the average of the normalized solar wind velocity was about 0.71 around a discontinuity, and associated KHI growth rate was about 0.4. Theoretically, KHI could be generated on the magnetopause by the velocity shear between this high-speed solar wind and the slow plasma velocity in the magnetosphere. Therefore, the mechanism that can generate the magnetopause surface waves is KHI even when these external condition changes were absent [e.g., *Fujimoto et al.*, 1998; *Hasegawa et al.*, 2004, 2006].

[73] Based on the locations of THEMIS-A and -C in GSM-XY and the time difference of the "complete" magnetopause crossings between by THEMIS-A and -C, we estimated the local speed of the magnetopause motion, and the amplitude of the surface waves. THEMIS-A and -C experienced first "complete" magnetopause crossings at 07:06 UT and 07:12 UT, respectively. Assuming that two probes have been stationary during 6 min, the surface wave amplitude reached 4.81 RE at the maximum, and local speed of the magnetopause motion was about 8.52 km/s. The obtained scale of surface wave amplitude was almost consistent with a rough thickness of KHI-unstable magnetopause as estimated by *Hasegawa et al.* [2004]. Because both THEMIS-A and -C experienced the magnetopause crossing at the inner and outer sites of the magnetopause, the surface waves were propagating along the line of THEMIS-A and -C. At 07:06 UT, THEMIS-A experienced "complete" outbound magnetopause crossing due to the surface waves, and simultaneous THEMIS-C was crossing "partially" the magnetopause. THEMIS-C experienced "complete" inbound magnetopause crossing at 07:12 UT due to an encounter of the surface wavefront passing through THEMIS-A. From 07:17 UT to 08:02 UT, THEMIS-C experienced the multiple magnetopause crossings. However, the wave amplitudes should be smaller than those at 07:06 UT and 07:12 UT

because THEMIS-A had not experienced "complete" magnetopause crossings until 08:03 UT.

11.2.2. Dawnside Near-Earth Magnetotail Responses

[74] THEMIS-D/-E observed the abrupt and transient magnetic field and plasma variations in the near-Earth magnetotail. The duration and amplitude of the variations were totally different from those observed by THEMIS-A. Furthermore, the background magnetic field of the B_z component and B_t of both THEMIS-D/-E gradually enhanced during the time interval of the variation, suggesting that THEMIS-D/-E observed the dipolarization. Simultaneous GOES-11 and -12 also observed the B_z enhancement due to the dipolarization, although associated striking global auroral activations were not found as well as the THEMIS-A's observational interval. Therefore, the abrupt and transient magnetic field and plasma variations observed by THEMIS-D/-E are caused by the substorm-like phenomena due to an IMF-B_x discontinuity encounter. Interestingly, magnetospheric plasma flow can be formed by the substorm-like phenomena. All components of the plasma velocity observed by THEMIS-E showed "bipolar-type" perturbations, indicating that the satellite observed "vortex-like" (circular) plasma flow structure. The duskward bursty plasma flow was observed in the V_y component of THEMIS-D, and the other V_x and V_z components were highly fluctuating. The substorm-like phenomena formed the complicated plasma flow structures because the plasma flow variations observed by THEMIS-D/-E were totally different even though the two probes were located very close to each other. Neither drastic plasma density nor temperature variations suggest that the plasma variations associated with the substorm-like phenomena were almost absent.

[75] The substorm-like phenomena triggered by the IMF-B_x discontinuity gave small-scale disturbances to the dawnside magnetotail as observed by THEMIS. Associated magnetic field and plasma variations clearly localized upon the dawnside near-Earth magnetotail, and their durations were also short-lived. From this result, the substorm-like phenomena induced by the IMF-B_x discontinuity occurred locally. Furthermore, its intensity (scale) was so moderate (small), being coincident with that the geomagnetic negative bay variations at the ground observatories were not negatively larger than -300 nT, which is a typical value of the geomagnetic field variation due to large-scale substorm.

12. Conclusion

[76] In this paper, based on the nine multisatellite observations, we examined the magnetic field and plasma responses in the magnetosphere to an encounter of an IMF-B_x discontinuity. The striking enhancement of the solar wind ram (dynamic) pressure and large-scale variation of the IMF-B_z structure were not associated with this discontinuity. This IMF-B_x discontinuity was a heliospheric current sheet which was separating the two high-speed solar wind streams with different velocity and magnetic polarity. THEMIS observed particular abrupt and transient magnetic field and plasma variations in the dawnside tail-flank magnetopause and near-Earth magnetotail. The magnetopause surface had large-scale waves due to Kelvin-Helmholtz instability (KHI). A velocity shear between high-speed solar wind streams and the stagnant plasma flows in the magnetosphere would generate KHI on the tail-flank magnetopause. THEMIS-A and -C, as located in the inner and outer sites of the tail-flank magnetopause, experienced the magnetopause crossings due to the induced waves. By instantaneously detecting the magnetosheath plasma through large-scale magnetopause surface waves, THEMIS-A observed resultant abrupt and transient magnetic field and plasma variations. On the other hand, the cause for the variations in the magnetic field and plasma as observed by THEMIS-D/-E comes directly from substorm-like phenomena induced by the IMF-B_x discontinuity. Interestingly, the magnetic field and plasma variations were localized upon the dawnside near-Earth magnetotail and their durations were also short-lived. This result explicitly suggests that the intensity (scale) of observed substorm-like phenomena was moderate (small).

[77] Based on the results obtained through this study, we found that the magnetotail can easily be varied by only one solar wind parameter's striking variation, even if the solar wind does not present significant variations, such as a sudden and/or long-term variation of the solar wind ram (dynamic) pressure and an encounter of the impulsive and/or long-term change of the IMF-B_z orientation. Furthermore, even the whole magnetosphere can be changed dramatically as a result.

[78] **Acknowledgments.** This work is supported by NSFC programs (40874086, 41031065) and partly by the National Key Research Project of China (2011CB811404). THEMIS was supported under NASA NAS5-02099. We thank N. F. Ness and D. J. McComas for the use of both MFI and SWE data of ACE, T. Nagai and S. Kokubun for the use of the Geotail MGF data, and D. J. Williams, R. W. McEntire, and A. T. Y. Lui for the use of the Geotail EPIC data. We thank A. Balogh and E. Lucek for the use of the Cluster FGM data via Coordinated Data Analysis Web site provided by NASA/GSFC. Moreover, we thank I. R. Mann, D. K. Milling, and the rest of the CARISMA team for providing the geomagnetic field data and World Data Center for Geomagnetism, Kyoto University, for the use of the data of the *AL*, *AU*, *AE* and $SYM-H$ indices. Also, we thank H. J. Singer for providing the GOES high-time resolution data and useful suggestions and comments for the evaluation and detailed analysis of the GOES data, and G. K. Parks and M. Brittnacher for the use of Polar UVI images. M. N. thanks Y. Miyashita (STEL/Nagoya University) and K. Liou (APL/Johns Hopkins University) for Polar UVI data processing and helping to make the data plot. CARISMA is operated by the University of Alberta, funded by the Canadian Space Agency. Wavelet software was provided by C. Torrence and G. Compo and is available at http://atoc.colorado.edu/research/wavelets/.

[79] Philippa Browning thanks the reviewers for their assistance in evaluating this paper.

References

Akasofu, S.-I., A. T. Y. Lui, and C.-I. Meng (2010), Importance of auroral features in the search for substorm onset processes, *J. Geophys. Res.*, *115*, A08218, doi:10.1029/2009JA014960.

Akasofu, S.-I., A. T. Y. Lui, and C.-I. Meng (2011), Reply to comment by Y. I. Feldstein, V. G. Vorobjev, and V. L. Zverev on "The importance of auroral features in the search for substorm onset process," *J. Geophys. Res.*, *116*, A02209, doi:10.1029/2010JA016079.

Angelopoulos, V. (2008), The THEMIS Mission, *Space Sci. Rev.*, *141*, 5–34, doi:10.1007/s11214-008-9336-1.

Aubry, M. P., C. T. Russell, and M. G. Kivelson (1970), Inward motion of the magnetopause before a substorm, *J. Geophys. Res.*, *75*(34), 7018–7031.

Auster, H.-U., et al. (2008), The THEMIS fluxgate magnetometer, *Space Sci. Rev.*, *141*, 235–264, doi:10.1007/s11214-008-9365-9.

Baker, K. B., and S. Wing (1989), A new magnetic coordinate system for conjugate studies at high latitudes, *J. Geophys. Res.*, *94*(A7), 9139–9143, doi:10.1029/JA094iA07p09139.

Borovsky, J. E., and M. H. Denton (2006), Differences between CME-driven storms and CIR-driven storms, *J. Geophys. Res.*, *111*, A07S08, doi:10.1029/2005JA011447.

Denton, M. H., J. E. Borovsky, R. M. Skoug, M. F. Thomsen, B. Lavraud, M. G. Henderson, R. L. McPherron, J. C. Zhang, and M. W. Liemohn (2006), Geomagnetic storms driven by ICME- and CIR-dominated solar wind, *J. Geophys. Res.*, *111*, A07S07, doi:10.1029/2005JA011436.

Fairfield, D. H., A. Otto, T. Mukai, S. Kokubun, R. P. Lepping, J. T. Steinberg, A. J. Lazarus, and T. Yamamoto (2000), Geotail observations of the Kelvin-Helmholtz instability at the equatorial magnetotail boundary for parallel northward fields, *J. Geophys. Res.*, *105*(A9), 21,159–21,173.

Farris, M. H., S. M. Petrinec, and C. T. Russell (1991), The thickness of the magnetosheath: Constraints on the polytropic index, *Geophys. Res. Lett.*, *18*(10), 1821–1824.

Feldstein, Y. I., V. G. Vorobjev, and V. L. Zverev (2011), Comment on "The importance of auroral features in the search for substorm onset process" by S.-I. Akasofu, A. T. Y. Lui, and C.-I. Meng, *J. Geophys. Res.*, *116*, A02208, doi:10.1029/2010JA016064.

Fujimoto, M., T. Terasawa, T. Mukai, Y. Saito, T. Yamamoto, and S. Kokubun (1998), Plasma entry from the flanks of the near-Earth magnetotail: Geotail observations, *J. Geophys. Res.*, *103*(A3), 4391–4408.

Gosling, J. T., M. F. Thomsen, S. J. Bame, and C. T. Russell (1986), Accelerated plasma flows at the near-tail magnetopause, *J. Geophys. Res.*, *91*(A3), 3029–3041.

Hasegawa, H., M. Fujimoto, T.-D. Phan, H. Rème, A. Balogh, M. W. Dunlop, C. Hashimoto, and R. TanDokoro (2004), Transport of solar wind into Earth's magnetosphere through rolled-up Kelvin-Helmholtz vortices, *Nature*, *430*(12), 755–758, doi:10.1038/nature02799.

Hasegawa, H., M. Fujimoto, K. Takagi, Y. Saito, T. Mukai, and H. Rème (2006), Single-spacecraft detection of rolled-up Kelvin-Helmholtz vortices at the flank magnetopause, *J. Geophys. Res.*, *111*, A09203, doi:10.1029/2006JA011728.

Keika, K., et al. (2009), Substorm expansion triggered by a sudden impulse front propagating from the dayside magnetopause, *J. Geophys. Res.*, *114*, A00C24, doi:10.1029/2008JA013445.

Kepko, L., and H. E. Spence (2003), Observations of discrete, global magnetospheric oscillations directly driven by solar wind density variations, *J. Geophys. Res.*, *114*(A6), 1257, doi:10.1029/2002JA009676.

Kepko, L., H. E. Spence, and H. J. Singer (2002), ULF waves in the solar wind as direct drivers of magnetospheric pulsations, *Geophys. Res. Lett.*, *29*(8), 1197, doi:10.1029/2001GL014405.

Kokubun, S., R. L. McPherron, and C. T. Russell (1977), Triggering of substorms by solar wind discontinuities, *J. Geophys. Res.*, *82*(1), 74–86, doi:10.1029/JA082i001p00074.

Lui, A. T. Y., et al. (2008), Near-Earth substorm features from multiple satellite observations, *J. Geophys. Res.*, *113*, A07S26, doi:10.1029/2007JA012738.

Mann, I. R., et al. (2008), The upgraded CARISMA magnetometer array in the THEMIS era, *Space Sci. Rev.*, *141*, 413–451, doi:10.1007/s11214-008-9457-6.

Matsuoka, H., K. Takahashi, K. Yumoto, B. J. Anderson, and D. G. Sibeck (1993), Observation and modeling of compressional Pi3 magnetic pulsations, *J. Geophys. Res.*, *100*(A7), 12,103–12,115.

McFadden, J. P., C. W. Carlson, D. Larson, V. Angelopoulos, M. Ludlam, R. Abiad, B. Elliott, P. Turin, and M. Marckwordt (2008), The THEMIS ESA plasma instrument and in-flight calibration, *Space Sci. Rev.*, *141*, 277–302.

Meng, C.-I., and K. Liou (2004), Substorm timings and timescales: A new aspect, *Space Sci. Rev.*, *113*, 41–75.

Pu, Z.-Y., and M. G. Kivelson (1983a), Kelvin-Helmholtz instability at the magnetopause: Solution for compressible plasmas, *J. Geophys. Res.*, *88*(A2), 841–852.

Pu, Z.-Y., and M. G. Kivelson (1983b), Kelvin-Helmholtz instability at the magnetopause: Energy flux into the magnetosphere, *J. Geophys. Res.*, *88*(A2), 853–861.

Russell, C. T., and R. C. Elphic (1978), Initial ISEE magnetometer results: Magnetopause observations, *Space Sci. Rev.*, *22*, 681–715.

Saito, T., K. Yumoto, and Y. Koyama (1976), Magnetic pulsation Pi 2 as a sensitive indicator of magnetospheric substorm, *Planet. Space Sci.*, *24*(11), 1025–1029.

Samsonov, A. A., D. G. Sibeck, and J. Imber (2007), MHD simulation for the interaction of an interplanetary shock with the Earth's magnetosphere, *J. Geophys. Res.*, *112*, A12220, doi:10.1029/2007JA012627.

Sckopke, N., G. Paschmann, G. Haerendel, B. U. Ö. Sonnerup, S. J. Bame, T. G. Forbes, E. W. Hones Jr., and C. T. Russell (1981), Structure of the low-latitude boundary layer, *J. Geophys. Res.*, *86*(A4), 2099–2110, doi:10.1029/JA086iA04p02099.

Shue, J.-H., et al. (1998), Magnetopause location under extreme solar wind conditions, *J. Geophys. Res.*, *103*(A8), 17,691–17,700.

Sibeck, D. G. (1992), Transient events in the outer magnetosphere: Boundary waves or flux transfer events?, *J. Geophys. Res.*, *97*(A4), 4009–4026.

Sibeck, D. G., and M. F. Smith (1992), Magnetospheric plasma flows associated with boundary waves and flux transfer events, *Geophys. Res., Lett.*, *19*(19), 1903–1906.

Sibeck, D. G., G. L. Siscoe, J. A. Slavin, E. J. Smith, B. T. Tsurutani, and S. J. Bame (1985), Magnetic field properties of the distant magnetotail magnetopause and boundary layer, *J. Geophys. Res.*, *90*(A10), 9561–9575.

Sonnerup, B. U. Ö., and L. J. Cahill Jr. (1967), Magnetopause structure and attitude from Explorer 12 observations, *J. Geophys. Res.*, *72*(1), 171–183.

Spreiter, J. R., A. L. Summers, and A. Y. Alksne (1966), Hydromagnetic flow around the magnetosphere, *Planet. Space Sci.*, *14*(3), 223–250, doi:10.1016/0032-0633(66)90124-3.

Takagi, K., C. Hashimoto, H. Hasegawa, M. Fujimoto, and R. TanDokoro (2006), Kelvin-Helmholtz instability in a magnetotail flank-like geometry: Three-dimensional MHD simulations, *J. Geophys. Res.*, *111*, A08202, doi:10.1029/2006JA011631.

Torr, M. R., et al. (1995), A far ultraviolet imager for the International Solar-Terrestrial Physics Mission, *Space Sci. Rev.*, *71*(1–4), 329–383, doi:10.1007/BF00751335.

Torrence, C., and G. P. Compo (1998), A practical guide to wavelet analysis, *Bull. Am. Meteorol. Soc.*, *79*, 61–78.

Tsurutani, B., and X. Y. Zhou (2003), Interplanetary shock triggering of substorms: Wind and Polar, *Adv. Space Res.*, *31*(4), 1063–1067, doi:10.1016/S0273-1177(02)00796-2.

Tsyganenko, N. A. (1995), Modeling the Earth's magnetospheric magnetic field confined within a realistic magnetopause, *J. Geophys. Res.*, *100*(A4), 5599–5612.

Wang, C., T. R. Sun, X. C. Guo, and J. D. Richardson (2010), Case study of nightside magnetospheric magnetic field response to interplanetary shocks, *J. Geophys. Res.*, *115*, A10247, doi:10.1029/2010JA015451.

Wilken, B., Q.-G. Zong, T. Doke, T. Mukai, T. Yamamoto, G. D. Reeves, K. Maezawa, S. Kokubun, and S. Ullaland (1998), Substorm activity on January 11, 1994: Geotail observations in the distant tail during the leading phase of a corotating interaction region, *J. Geophys. Res.*, *103*, 17,671–17,689.

Williams, D. J., R. W. McEntire, C. Schlemm II, A. T. Y. Lui, G. Gloeckler, S. P. Christon, and F. Gliem (1994), Geotail energetic particles and ion composition instrument, *J. Geomagn. Geoelectr.*, *46*, 39–57.

Wiltberger, M., R. E. Lopez, and J. G. Lyon (2003), Magnetopause erosion: A global view from MHD simulation, *J. Geophys. Res.*, *108*(A6), 1235, doi:10.1029/2002JA009564.

Zhou, X., and B. Tsurutani (2001), Interplanetary shock triggering of nightside geomagnetic activity: Substorms, pseudobreakups, and quiescent events, *J. Geophys. Res.*, *106*(A9), 18,957–18,967, doi:10.1029/2000JA003028.

Zuo, P. B., F. S. Wei, X. S. Feng, and F. Yang (2007), The relationship between the magnetic cloud boundary layer and the substorm expansion phase, *Sol. Phys.*, *242*, 167–185, doi:10.1007/s11207-007-0407-3.

Zuo, P. B., F. S. Wei, X. S. Feng, X. J. Xu, and W. B. Song (2010), Magnetic cloud boundary layer of 9 November 2004 and its associated space weather effects, *J. Geophys. Res.*, *115*, A10102, doi:10.1029/2009JA014815.

V. Angelopoulos, Institute of Geophysics and Planetary Physics, University of California, Los Angeles, CA 90095, USA. (vassilis@igpp.ucla.edu)

H.-U. Auster, Institut für Geophysik und Extraterrestrische Physik, Technische Universität, Mendelssohnstr. 3, D-38106 Braunschweig, Germany. (uli.auster@tu-bs.de)

C. W. Carlson, Space Sciences Laboratory, University of California, 7 Gauss Way, Berkeley, CA 94720-7450, USA. (cwc@ssl.berkeley.edu)

S.-Y. Fu, M. Nowada, and Z.-Y. Pu, Institute of Space Physics and Applied Technology, School of Earth and Space Sciences, Peking University, Beijing 100871, China. (suiyanfu@pku.edu.cn; nowada@pku.edu.cn; zypu@pku.edu.cn)

C.-H. Lin, Department of Electrical Engineering, Ching Yun University, Taoyuan 32097, Taiwan. (chlin@cyu.edu.tw)